Respective roles of the weathering profile and the tectonic fractures in the structure and functioning of crystalline thermo-mineral carbo-gaseous aquifers

Benoît Dewandel, Marina Alazard, Patrick Lachassagne, Vincent Bailly-Comte, Renaud Couëffé, Sandrine Grataloup, Bernard Ladouche, Sandra Lanini, Jean-Christophe Maréchal, Robert Wyns

Published in Journal of Hydrology 547 (2017) 690–707; http://dx.doi.org/10.1016/j.jhydrol.2017.02.028

Respective roles of the weathering profile and the tectonic fractures in the structure and functioning of crystalline thermo-mineral carbo-gaseous aquifers

B. Dewandel[a], M. Alazard[b,c], P. Lachassagne[c], V. Bailly-Comte[a], R. Couëffé[d], S. Grataloup[d], B. Ladouche[a], S. Lanini[a], J-C. Maréchal[a], R. Wyns[d]

[a] BRGM, Water Environment & Ecotechnologies Division, 1039 rue de Pinville, F-34000 France Montpellier, France. b.dewandel@brgm.fr
[b] GEOTOP, Département des Sciences de la Terre et de l'atmosphère, UQAM, Montréal, Canada. alazard.marina@uqam.ca
[c] Water Institute by Evian, Evian-Volvic World, Danone Waters, Evian-les-Bains, France. patrick.lachassagne@danone.com
[d] BRGM, Geology Department, 3 Avenue Claude-Guillemin, BP 36009, 45060 Orléans, France

Abbreviations: BRGM: Bureau de Recherches Géologiques et Minières; CGG: Compagnie Générale de Géophysique; CTMCG: Crystalline Thermo-Mineral and Carbo-Gaseous; EMMA: End-Member Mixing Analysis; GW: GroundWater; MARTHE: Modelling of Aquifers with Rectangular grid in Transient state for Hydrodynamic calculations of hEads and flows; PCA: Principal Component Analysis

1. Introduction

Thermo-mineral and carbo-gaseous hydrosystems are well known for their economic importance and are exploited for centuries for thermal and spa activities. Sparkling natural mineral waters are bottled in Europe since the early XVIIth century (Lopoukhine, 1998) and constitute a dynamic industry (e.g. Renac et al., 2009; Cinti et al., 2014). These hydrosystems are associated with specific geological structures, such as faults and fractures in crystalline bedrock, allowing deep (hot) fluids and/or gases travelling to the surface. Case studies are scarcer in geological sedimentary context where gases fluxes are often masked by the sediments. These high heat/gas flow areas are generally associated with recent volcanism and/or extensional tectonics such as graben or back-arc basins (e.g. Barnes et al., 1984; Kerrick et al. 1995; Matthews et al. 1987; Weinlich 2005).

Despite their economic importance, due to their structural complexity, crystalline thermo-mineral and carbo-gaseous (CTMCG) hydrosystems are rarely characterized in detail (see nevertheless for instance Maréchal et al., 2014). In the absence of a better alternative, groundwater fluxes are often considered to be limited to fractures and faults related to the tectonic regime (e.g. Forster and Smith 1989, Stober and Bucher 1999) in hydraulically active faults whose geometry is rarely known. Moreover, in many descriptions, faults are assimilated to pervious structures, often without any hydrodynamic argument, even if several studies demonstrate that they are often impervious due to rock crushing and various kind of sealing materials (e.g. Mohamed and Worden, 2006; Lachassagne et al., 2011; Petrella et al. 2015; Tokan-Lawal et al. 2015).

However, groundwater flow in crystalline aquifers is not limited to tectonic fractures. Such aquifers more commonly derive their hydrodynamic properties from weathering processes (Acworth, 1987; Chilton and Foster 1995; Dewandel et al. 2006; Lachassagne et al., 2011), resulting in weathering profiles composed of several stratiform layers. From top to bottom, where not partially or totally eroded, they are i) several tens of metres thick unconsolidated saprolite layer and laminated saprolite layer, together forming the "regolith". Given its clayey–sandy composition, this superficial layer may have a high porosity (up to several percents, depending on the lithology of the mother rock) but a low hydraulic conductivity. ii) The underlying "fissured layer" (Lachassagne et al., 2011) that constitutes the transmissive part of the aquifer. It has been shown that its fracturing is induced by prolonged in-situ weathering processes, mostly as a consequence of the stresses induced by certain swelling minerals such as biotite (e.g. Wyns et al., 2004; Dewandel et al., 2006; Lachassagne et al. 2011). Below the weathering profile (saprolite + fissured layer), (iii) the fresh basement is only permeable where discontinuities (ancient tectonic fractures, joints, veins, dykes, lithological contacts,

etc.) induce locally a deepening of the weathering front and, consequently, the development of some pervious fractures along these ancient structures (Dewandel et al., 2011; Lachassagne et al., 2011).
Although the previously developed conceptual models based on groundwater flow through faults and tectonics fractures only can be relevant, the hydrodynamic properties of such fractured aquifers are rarely characterized in details, nor their geometry and functioning described in 3-D. Moreover, fissured layers of large extension are rather a generality in shallow crystalline aquifers, and faults are not always, or even rarely, permeable structures.
The aim of this work is to characterize in details a CTMCG hydrosystem associated with a peri-Alpine graben in order to understand its geological structure and hydrogeological functioning. A multidisciplinary approach is developed with various complementary methods: geological modelling with geophysics and geological data from outcrops and boreholes, hydrodynamic data, hydrochemistry, hydrogeological and geochemical modelling. The converging results allow conceptualization of the system. The strengths of this work rely, among others, on the high density of information, rarely available in such a context, and the transferability of the resultant conceptual scheme.

2. Material and methods

2.1. Study site. Location, geological and hydrogeological description of the study area

The CTMCG system of Saint-Galmier (Saint-Galmier, France) is located at the boundary between two distinct geomorphological and geological areas: the Forez plain to the West, with outcropping Oligocene to Quaternary sediments, and the Hercynian crystalline massif of the Monts-du-Lyonnais to the East (Figure 1), separated by a major roughly N-S oriented tectonic fault.
From a structural point of view, the Forez Plain is a N-S elongated graben, resulting from the Cenozoic rifting associated with an early stage of the Alpine orogenic event (Figure 1a). This extensive phase is highlighted by the normal faults bordering the plain on both sides (Figure 1b).
At Saint-Galmier, the N-S oriented border fault separates the Forez plain from the Monts-du-Lyonnais plutonic and metamorphic rocks. The city of Saint-Galmier lies on porphyritic calc-alkaline granite with biotite. The granite often appears weathered, both at outcrop and in boreholes, and shows:
i) an often thin layer of sandy saprolite, a clay-rich material with coarse sand-size clasts, mainly washed away by Plio-Quaternary erosion,
ii) a very thick laminated saprolite layer (from 15 m to more than 30 m-thick). This layer is constituted by a relatively consolidated highly weathered parent rock with a coarse sand-size clasts texture and a millimetre-scale dense horizontal lamination crosscutting the biggest minerals,
iii) and a fissured layer, observed from boreholes but rarely at the surface. This layer is characterized by several fractured zones with a depth-decreasing density. Some of these zones are filled with highly weathered materials similar to the sandy saprolite.
The rift-type basin of the Forez plain is a relic of the system of the Loire's Limagne that belongs to the European Cenozoic peri-Alpine grabens (Figure 1a). It is filled up with Late Eocene to Miocene clayey-sandy sedimentary deposits which can reach up to 800 m in the central part of the basin (Ech-Cherif El Khetani, 1996; Briot et al., 2001). Deposits are continental and show a strong spatial heterogeneity at the basin scale with:
i) a dominant clayey-conglomeratic and -sandy facies close to the borders and in the northern part, with piedmont facies inherited from border reliefs,
ii) claystone and marl dominant facies in the central and southern areas with floodplain and lake facies (Gerbe et al., 1998). Quaternary alluvium of the Loire River and its tributaries – both recent and old – covering the Forez plain are masking the Tertiary sediments described above (Figure 2).
Several sparkling natural mineral waters (NMW) are known around the basin, the south-eastern border fault of the graben (Figure 1) being the discharge point of the studied deep mineral carbo-gaseous system, the Saint-Galmier natural mineral water. The historical "Fontfort" spring (see location on Figure 4) was exploited since the Antiquity, and has been bottled at Saint-Galmier since 1837. The development of its commercial use, with the digging and exploitation of deep large

diameter wells, and then the drilling of borewells during the second half of the XXth Century, progressively lowered the piezometric level, and dried up the spring during the XIXth century. A new hydrodynamic steady state was reached during the XXth century, with now stable piezometric levels since several decades at least. As it is ancient, the previous unsteady state is not documented with data chronicles.

2.2. Methods and data

In this research, a multidisciplinary approach was applied to gather clues obtained from each method. Results from these complementary methods were compiled to conceptualize the aquifer structure and its functioning. These various methods are described here below.

a) Geological data (re)interpretation

Data from 254 boreholes (including 60 boreholes located in the narrow study area – Figure 1 and Figure 2) were analyzed for geological and structural interpretation. Additional geological, weathering and structural (e.g. fractures, joints and faults) observations were carried out on 27 outcrops and on a 70 m-deep cored drill (Figure 4). A simplified geological map with stratigraphic succession for the basin was also established by (re)analysing and confronting bibliographic data (e.g. Duclos, 1967; Duclos et al., 1974; Ech-Cherif El Kettani, 1996; Gerbe et al., 1998; Barbarin et al., 2012a & b; and Couëffé et al., 2014).

b) Geophysics

Six existing seismic profiles (CGG, 1990) covering the narrow study area were reprocessed and reinterpreted. A detailed geometrical analysis was performed on seismic reflectors to identify (i) the main stratigraphic unconformities and (ii) the vertical displacement of successive reflectors which are assumed to highlight tectonic discontinuities.

Stratigraphic attributions of seismic units were assigned on the basis of geometrical relationships between reflectors and validated by the calibration with sedimentary succession recognized at near subsurface in closest deep boreholes (17 boreholes with depth ranging between 70 and 350 m). Additionally, check-shot survey on Frarie borehole and analysis of P-wave velocities on samples (from 6 outcrops and the cored-well) were used to define mean interval velocities of each seismic unit and to calibrate the conversion from time seismic to depth geological sections.

The analysis of reflectors located below Cenozoic deposits highlights the existence of distinctive internal seismic units into the St-Galmier granite weathered layers. These distinctive units are characterized by reflection with bedded geometries that do not display sedimentary features. Their estimated thicknesses were compared to those defined from saprolite and fissured layers from borehole lithologs. The good consistency between thicknesses leads to consider that the distinguished of seismic units below Cenozoic sedimentary cover can be attributed with the St-Galmier granite layers of the weathering profile. Additional geophysical data (electrical resistivity profiles, gravimetric maps) were also used to constraint the geological scheme.

c) 3D-geological and structural model

Borehole logs and seismic profiles reinterpretation allowed identification of the main lithostratigraphical and structural elements of the area; i.e. faults, stratigraphic succession, geometry of sedimentary deposits, paleo-morphology of the Paleozoic substratum and geometry of its weathered layers. Two areas (Figures 1 and 2) were used for the construction of the geological model: the “narrow study area”, with a high density of data, and an “extended area” with scarcer data, but necessary to define a precise scheme at the boundaries of the “narrow area”.

These main geological and structural elements were gathered in a 3-D geometrical numeric model using the Geomodeller© software developed by BRGM and Intrepid Geophysics. Geomodeller© uses the co-kriging method for spatial interpolation (Lajaunie et al., 1997 ; Calcagno et al., 2006 ; Courrioux et al., 2006 ; Calcagno et al., 2008).

d) Hydrodynamics: pumping tests and airlift measurements

A total of 36 pumping tests is available within the “narrow area” (see Fig. 6), 24 were performed in the granite (in 18 different boreholes) and 12 in the Cenozoic deposits (11 boreholes). Test durations range from a few days to several months with flowrates between 1.2 and 13 m^3/h in the Tertiary sediments and between 1.8 and 40 m^3/h in the granite.

Data interpretation was conducted in two phases: analysis of the tests and modelling. After normalizing the drawdown curves according to pumping rate changes, the log–log diagnostic plot developed by Bourdet et al. (1983) was used. This analysis of derivative drawdown facilitates the identification of a conceptual model without preliminary or ‘‘a priori” hypothesis on the aquifer’s structure. Derivative curves were computed numerically based on the algorithm proposed by Bourdet et al. (1989) and type curves were used for determining flow regimes (Bourdet et al., 1983, 1989; Ehlig-Economides, 1988; Deruyck et al., 1992; Spane and Wurstner, 1993; Renard, 2005; Renard et al., 2009; Dewandel et al., 2014). The diagnosis allows identifying the properties of the borehole (e.g. borehole storage, skin effects), of the aquifer (e.g. isotropy/anisotropy, fractures, dual porosity), its geometry (boundaries of various types), the possible relationships with other aquifers (e.g. leakage), etc. Then, the mathematical model respecting the identified flow-regimes was used to compute drawdown and to estimate hydrodynamic parameters. To this end a simultaneous double fitting on both drawdown and derivative drawdown is necessary. This methodology has been, for example, successfully applied for the hydrodynamic characterization of hard rock aquifers (Dewandel et al., 2011, 2014; Roques et al., 2014; Maréchal et al., 2014).

According to the diagnoses of the Saint-Galmier’s pumping tests (see the “results” section), two horizontal multi-layers aquifer models that respect the identified flow-regimes were used: one considers that the piezometric variation in the overlying aquifer due to leakage is negligible (model derived from Hantush, 1961); the other considers that the piezometric level decreases in the upper aquifer because of pumping in the deeper aquifer (model derived from Hunt and Scott, 2007). As diagnoses showed evidences of no-flow boundaries, the models also consider up to 4 orthogonal no-flow boundaries (i.e. up to a laterally closed reservoir). A compartmentalized aquifer model, i.e. the pumped aquifer is laterally limited by two other aquifers with various hydrodynamic properties (Dewandel et al., 2014), was also used.

Air-lift flow measurements carried out during the drilling of down-to-the-hole-hammer boreholes were treated statistically particularly to provide the depth of productive fracture zones (Maréchal et al., 2004; Dewandel et al., 2005; Courtois et al., 2010, Roques et al., 2016). We compiled air-lift data from 29 boreholes (measurements every 3 metres in average) and also added the depth of productive fracture zones deduced from flowmeter measurements (every meter in average) in 4 other boreholes from which air-lift flows were not available. 195 productive zones were identified. The discharge and location of the productive zones were referenced with respect to the interface between the saprolite and the granite’s underlying fissured layer in order to explore if there is any vertical trend of productive fractures distribution in the fissured layer (e.g. Courtois et al., 2010).

e) Piezometric level and discharge monitoring

As the natural mineral water is pumped for bottling, piezometric level and borehole pumping rate are recorded at a hourly time step in the 10 abstraction boreholes, equipped either within the granite or within the Tertiary sedimentary aquifers, since their construction, and in 14 unpumped observation boreholes since 2010 (although previous monitoring was also existing). In the granite, six nested piezometers in the weathering profile were drilled and equipped in 2009. Several campaigns of piezometric measurements, including non-monitored wells, are also available across the studied area. Discharge of the Coise stream is also measured at a hourly time step.

f) Geochemistry

Hydrochemical parameters of the abstraction boreholes are monitored weekly. In addition, groundwater punctual analyses for major ions are available from 1962 to 1998 on 67 other boreholes from the Saint-Galmier area, and 10 additional mineralized water samples at the scale from the Forez plain area. A sampling campaign was also performed in 2010: 22 groundwater and surface water (Coise stream) samples were analysed for major ions. This geochemical database was used to define the Saint-Galmier NMW geochemical facies and its main characteristics as compared to other NMW types found locally and regionally. Water type classification was performed using Piper diagrams, biplots, Principal Component Analysis (PCA) and End-Member Mixing Analysis (EMMA) following the Christophersen and Hooper’s method (1992). Distinction among groundwater characteristics was defined using the computation of the sodium-pole indicator: Sodium-pole (%) = ([HCO_3^-] – ([Ca^{2+}] +

$[Mg^{2+}]))/ [HCO_3^-]$ with element concentrations expressed in meq/L. This indicator, varying between 0 and 1, allows a clear distinction between Na and Ca groundwater types, regardless of the total mineralization and the HCO3- content.

EMMA was used to determine proportions of end-members contributing to the NMW pumped in the abstraction boreholes. 580 data (major ions) from January 2000 to December 2012 were used. For each abstraction borehole, the hydrochemical time series and the potential end-members, i.e. water samples from the geochemical database, were standardized for all major ions using the mean and standard deviation of the hydrochemical time series. The main steps can be summed up as follow (see Burns et al., 2001 for details), each water sample being described in *n*-dimensions, *n* being the number of ions used for the EMMA: i. From these *n*-dimensions, a PCA is used to find a new 2-D space in which most of the variance of the chemistry dataset is kept; ii. The potential end-members are plotted in this new space, which allows graphically selection of up to 3 water samples to characterise the water chemistry pumped in the exploited borehole; iii. The relative position of these 3 end-members compared to the water samples from the abstraction borehole allows quantifying 3 mixing ratios, which are used to re-compute the series of the *n* major ions; iv. A statistical (least square linear regression) goodness of fit is computed to validate the choice of the end-members. If needed, steps 2 and 3 are repeated until the best fit is obtained.

From these approaches, different poles of groundwater were identified and indicators were developed to allow mixing rate quantification within each groundwater body.

g) Numerical modelling of an aquifer compartment

A deterministic hydrogeological model of the best known aquifer compartment (A3) was developed using the MARTHE_7.4© BRGM finite differences code (Thiéry, 1990, 2010). The 2D multilayer model comprises the four main layers i.e. the sedimentary deposits, a confining layer, the saprolite and the fractured layers of the granite). The modeled area is a rectangle of 2.05 km by 1.66 km (Figure 12) composed of 1353 square cells (50 x50 m) per layer. The model solves in steady state both hydrodynamic and mass transport equations. Boundary conditions were defined according to the available knowledge synthetized in the conceptual model. The main objective of this modelling is to validate the hydrogeological conceptual model for this compartment, to confirm and spatialize the geochemical results about mixing rates, and to locate the deep fractures providing deep highly mineralized fluid.

h) Synthesis and hydrogeological conceptual model

All the information obtained from these various approaches was compiled and synthesized in a realistic hydrogeological conceptual model that explains the geological structure and hydrogeological functioning of the aquifer system. Each method provides clues which individually may not be significant but, when converging towards a similar scheme, they allow building up a consistent hydrogeological conceptual model.

3. Results and interpretation

3.1. Geological model

3.1.1. Lithological model

The main geological layers described in the lithological model are i) Quaternary deposits (alluvium and colluvium); ii) Cenozoic sedimentary deposits with distinction between syn-rift and post-rift units; weathered granite including iii) the saprolite (sandy regolith and laminated layer) and iv) the underlying fissured layer.

The geological map (Feybesse et al., 1996) shows the stratigraphic sequence from top to bottom: i) the recent and ancient Quaternary alluvium and colluvium covering the Forez plain until the foothills of the crystalline massifs of the Monts du Lyonnais and ii) the Cenozoic deposits of the post-rift and syn-rift series (see below their description), the first ones forming a narrow band along the contact between the Forez plain and the Monts du Lyonnais (Figure 2), iii) the crystalline massifs of the Monts du Lyonnais mainly formed by the plutonic St-Galmier's granite and its weathering facies.

The seismic profiles (Figure 3), calibrated using borehole geological logs, cores and P-waves measurements, were used to locate the thickness of the sedimentary cover and to discriminate the

unconsolidated saprolite from the laminated layer within the sandy regolith. The main fractured zone within the fissured layer (upper part of the fissured layer) was readily identified on seismic profiles (Figure 3). In the Cenozoic sedimentary deposits an internal unconformity separating syn-rift and post-rift series (Duboeuf et al.,1991) divides the Cenozoic sediments into two units with differing hydraulic properties: (i) a low hydraulic conductivity mostly clayey Late Eocene - Oligocene "synrift" series and ii) a Miocene (post-Aquitanian) "post-rift" series characterized by a higher hydraulic conductivity due to its mostly clayey-sandy to sandy composition.

3.1.2. Structural model

From the reinterpretation of geological and geophysical data, the main structural elements identified and located are: i) mainly normal faults highlighted by shifts of seismic reflectors in the synrift series that do not affect post-rift deposits; ii) strike-slip accidents, inducing only small shifts on seismic reflectors and characterized by complex geometries ascribed to flower structures; iii) depocenters of the synrift deposits; iv) positive palaeomorphologies of the top of the Paleozoic bedrock, often corresponding to hanging wall related to main normal faults; v) zones of higher fracture density in the granite (for which reflectors belonging to the weathering profile are more discontinuous and of lower frequency).

A structural model was built locating the two main types of faults (Figure 4): i) normal faults sealed by the post-rift deposits and ii) on the eastern edge, normal faults affecting both the synrift and post-rift series also related to the Cenozoic extension but being lately reactivated.

3.1.3. The 3-D geological model

The 3-D geological model, built with the Geomodeller© software (Figure 4), allowed the spatial representation of the faults and the isohypses of the main geological layers and interfaces, i.e., from bottom to top: undifferentiated unweathered granite and fissured layer, laminated layer, unconsolidated saprolite, syn-rift and post-rift deposits. Quaternary sediments, as they are very thin, were integrated in the post-rift layer. From a hydrogeological standpoint, this model informs the depth and geometry (top) of the potential aquifers in the granite and location of faults that may convey deep mineral water and CO_2 to these aquifers. The model shows where aquifers (the granite's fissured layer, aquifers within Cenozoic layers) can laterally be placed by faults opposite to impervious formations. Finally, it allows assessing the spatial extension of the low hydraulic conductivity syn-rift Cenozoic deposits that may act as aquitards as well as the spatial extension of post rift sediments that may allow a connection between granite aquifers and the subsurface.

3.2. Hydrodynamics

a) Interpretation of pumping tests

Data from36 pumping tests were analysed and modelled. To illustrate, Figure 5 shows the type curves and derivative curves of pumping tests performed on the A3 borehole as well as those corresponding to A1 and A2 boreholes located at 42.5 m and 19.7 m from A3, respectively. These three wells are located in the granite under the sedimentary cover (about 30 m thick) and are hydraulically connected. The thickness of the saprolite is variable, 41 m for A1, 10 m for A2 and 52 m in A3. Drawdown curves are shifted because of the well effects of each borehole (wellbore, skin, head losses). However their derivatives are characterized with a similar pattern, demonstrating that these three boreholes belong to the same granite aquifer. The succession of flow behaviours – (i) radial flow, (ii) linear flow, (iii) leakage, and (iv) pseudo-steady state flow with a slope of 1 -, respectively shows (i) that the granite aquifer has a transmissivity ranging between 1.4 and 1.8×10^{-3} m^2/s, (ii)&(iv) that it is limited in space by several impervious limits and that its shape is a priori "rectangular" and relatively elongated. Additionally (iii) it shows evidence of leakage quite surely from an overlying aquitard (saprolite and/or post-rift sediments). The used model (Hunt and Scott (2007) model with no-flow boundaries) successfully matches the observed drawdowns.

Derivative curves from 34 tests, regardless of the geological formation, exhibit similar behaviours i.e. an aquifer limited in space by 2 to 4 impervious limits (symbols B, C and D in Figure 6). Depending on the duration of the tests and on the distance to the limits, all limits were not necessarily identified, as well as leakage effects. Only one test (Charpinière borehole; Cenozoic deposits) shows a different diagnosis: a laterally compartmentalized aquifer.

The bore wells where 4 impervious limits were reached belong to aquifer "compartments" which surface area was then estimated (with an accuracy depending on the reliability of the estimate of the storage coefficient). All computed surface areas are of the order of one square kilometre. Each of these so-identified no-flow boundaries was then successfully attributed to one of the faults from the structural scheme (Figure 6). They appear to correspond with the graben faults, i.e. N-S and N130 (Figure 9). Therefore, these faults appear to have a low permeability. This is due either to impervious fault gouge, or because of the contact between permeable (fissured granite) and low-permeability formations (Cenozoic deposits, saprolite), due to fault throws.

b) Air-lift data analysis

Figure 7a shows the average air-lift flow and flowmeter measurements from boreholes, according to the depth below the bottom of the saprolite. No flowrate was observed in the saprolite layer. Figure 7b provides the density of productive fracture zones according to the depth. The percentage of available data according to depth is also presented (Figure 7c). Statistics from Figures 7a and 7b are considered representative at a given depth where at least 30% (Dewandel et al., 2005) of the data are available, as not all wells reach the deepest depths. Consequently, data below 150-175 m below the saprolite bottom are not considered significant. The productive fractures' density (Figure 7b) was corrected according to this observation density (for each depth interval, corrected density equals raw density multiplied by the percentage of observation).

The average of the total air-lift flowrate by borehole is 30 m^3/h, with 30% of the boreholes reaching higher flowrates, which is rather high for cristalline rock aquifers. Cumulated average flowrate increases with depth below the saprolite in the first 100-125 metres below the base of the saprolite, then tends to stabilize down to 150-175 m and becomes erratic deeper because of the lack of data. Similarly and logically, the productive fracture density is the highest in this 100-125 m interval; this was also observed on raw data, i.e. not corrected from observation density (not shown on Figure 7). The tickness of the fissured layer of the granite aquifer is then about 100 to 125 m (see also Figure 3).

c) Hydrodynamic properties of the aquifers (from pumping tests)

This 100-125 m thick granite aquifer shows high transmissivity values for a fractured granite aquifer (~ 10^{-3} m^2/s, Figure 8). This is about 10 to 100 times the values usually expected for such a lithological context. The transmissivity of the granite aquifer is lower (down to 10^{-5} m^2/s) in the deepest part of the hydrosystem located in the western part of the study area under a thick sedimentary cover (Figure 8); this result will be discussed later. Storage coefficients range between 10^{-3} and $5x10^{-5}$.

The granite aquifers also exhibit minor leakage effects (E symbol on Figure 6) that are attributed to the low hydraulic conductivity Cenozoic sediments, and/or to the saprolite layer, and particularly its laminated bottom. The estimated hydraulic conductivity of leaky layers is about 10^{-9}-10^{-8} m/s.

The transmissivity of Cenozoic deposits aquifers ranges from $2x10^{-5}$ to $8x10^{-3}$ m^2/s. Much more than for granite aquifers, their hydrodynamic parameters are highly heterogeneous and they are compartmented, due to the small lateral and vertical extension of sand bars. Despite its estimation was limited by the absence of piezometers, the spatial extension of these compartments, of about 0.1 km^2 each, appears to be lower than the one of the granite aquifers. Leakage effects (10^{-10}-10^{-7} m/s) were found for a few pumping tests, highlighting the multi-layered structure of the Cenozoic deposits.

3.3. Piezometric data

The piezometric data (Figure 9) logically show that, in each exploited aquifer compartment, the groundwater flows converge towards the abstraction borehole (logically, only one well is pumped in each aquifer compartment). This scheme is particularly clear in the A3 compartment where a detailed piezometric data set is available. The high piezometric differences between the different aquifer compartments confirm the low permeability of the boundaries that limit them that were identified and located from both pumping tests and the geological model.

A "Multiple Input Single Output" temporal analysis of the piezometric time series (e.g. Maréchal et al., 2014) from the granite aquifer (fissured layer) was used to discriminate the impact of pumping, rainfall and water level from the Coise stream and sedimentary formations. Impulsional responses associated to each input highlight that piezometric variations in the granite aquifer are i) weakly

related to the climatic variability and water levels in sedimentary formations, and not at all to the Coise stream, ii) quite exclusively influenced by the pumping rate in each compartment and iii) not influenced by the pumping rate changes in adjacent compartments, which confirms the no-flow boundaries between them.

3.4. Geochemical tools

3.4.1 GW chemical facies

The spatial distribution of GW mineralization is highly variable in space, at both local (Saint-Galmier) and regional (Forez plain) scale, ranging from few hundreds to more than 6000 µS/cm. Graphical major ions analysis using Piper diagrams and biplots were first used to check if the lithology of the GW reservoir (Cenozoic deposits/unconsolidated saprolite/fractured granite) could explain the GW chemical facies. No relationship was found, showing that local water-rocks interaction is not the main process that explains the GW chemistry. Mixing processes can thus be proposed, which implies to identify different poles to describe the mineralization, regardless of the nature of the geological reservoir.

Highly mineralized water (>4000 µS/cm) is mainly of HCO3-Na type in the Forez plain but mineralized water of HCO3-Ca-Mg type can also be found in the Saint-Galmier area. This is why the Ca/Na ratio was used to identify the relative contribution of these two mineralized poles. A third type of GW is defined by its low mineralization (<500 µS/cm), which is representative of aquifers that are not fed by deep mineral inputs. The 2 mineralized poles are clearly highlighted on Figure 10 where the Ca/Na ratio is compared to the electrical conductivity: Ca-Mg-type for which the Ca/Na ratio is higher than 0.6 and Na-type for which the Ca/Na ratio is below 0.2. Low-mineralized water (<500 µS/cm) appears as a dilution pole and shows a large range of Ca/Na ratio. Mixing processes occurring between the different groundwater poles can thus explain the variability of chemical facies and electrical conductivities of groundwater within the system (Figure 10).

3.4.2. Spatial analysis

As the samples are well distributed across the area, the sodium-pole indicator helps in characterizing the spatial representation of the sodium pole within each aquifer compartment through kriging interpolation and also to compare the chemistry of the various compartments (Figure 13). In this representation, the groundwater samples from the “dilution pole” were excluded to focus on the location of the input of deep mineralized water within the aquifer system. Then, the spatial distribution of the chemical facies is consistent with the aquifer compartments previously identified. Figure 13 shows that the Na-type water is associated with the mineralized province observed around Violes where EC reaches 5000 µS/cm, whereas the mineralized area of Pétillante, Généreuse and the surrounding boreholes also shows highly mineralized water (>5000 µS/cm) associated to a relatively strong calcium facies. The area of the Ca-Mg water type (Ca/Na ratio > 0.6) therefore appears to be moderately mineralized compared to Na-type groundwater observed elsewhere. This Ca-Mg water type also remains spatially limited, in the Saint-Galmier area.

Beyond the spatial repartition of the different types of mineralized water within specific compartments based on the former analysis, the distribution of electrical conductivities highlights the distribution of the groundwater from the dilution pole within compartments. It is clearly visible that the least mineralized groundwater (e.g. Aubignat, Cote Rouge and Hippodrome) is found in specific aquifers compartments (Figure 13). Mineralization gradients in aquifer compartments are induced by pumping boreholes location as well as the location of the sources of deep mineral water and dilution poles. To precisely identify these locations, deterministic modelling was performed on the best known compartment (A3; cf. §3.5).

3.4.3. Temporal analysis.

Chemical data from the A3 compartment were analysed with the EMMA statistical method. Firstly, a PCA (Principal Component Analysis) was performed using the 6 major ions HCO_3^-, Ca^{2+}, Mg^{2+}, Na^+, Cl^- and NO_3^-. 84% of the total variance was explained by 2 factorial axes. The F1 axis, linked to overall mineralization, highlights the mixing processes between deep mineralized groundwater and the dilution pole in the A3 borehole (Figure 10) and within the A3 compartment. The best candidate for the “deep” pole was the composition of the A3 borehole groundwater in 1985 (i.e. just after its

drilling, at the beginning of its abstraction). There was no clear chemical distinction between dilution pole from the saprolite and from the Cenozoic sedimentary aquifer, but a mixing of two distinct dilution end-members is needed. The best fit was given using two water samples from boreholes drilled in the unconsolidated saprolite.

Contribution rates from the deep pole and the dilution pole were simulated over the time using the time series of chemistry of A3 groundwater and the corresponding pumping rates (Figure 11). The EMMA allows reproducing the hydrochemical time series of the 6 major ions with a correlation coefficient between 0.86 and 0.95. The deep contribution is relatively stable. It highlights that pumped water in A3 is composed of about 60% of the deep component and 40% of the dilution pole. This result is used to better constrain the deterministic modelling of the A3 compartment (cf.§ 3.5.3).

3.5. Deterministic modelling of the A3 compartment

The calibration of the numerical model was carried out by simulating the system both under natural conditions before pumping started and under abstraction in both granite (abstraction of 18 m^3/h in A3) and Cenozoic aquifers. The main criteria to assess the validity of the model were i) the location of the the historical Fontfort spring that was flowing out from this compartment (Figure 4) in the natural state and its absence after several centuries of borehole abstraction, ii) the consistency of the calibrated parameters and boundary conditions compared to values of reference data (i.e. permeability, recharge, deep mineralized water flow) and iii) the calculated groundwater levels compared with available measurements.

3.5.1. Boundary conditions and hydraulic properties

To reproduce the East-West regional flow in the Cenozoic formations, a constant hydraulic head condition equal to the topographic level minus 1.5 metres was imposed on the cells of the western limit of the model. For the other lateral boundaries of the model, it is assumed that the modelled area is sufficiently large compared to that of the A3 reservoir for boundary conditions not to affect the flows in the A3 area. A no-flow condition is thus imposed along the perimeter of the modelled area for all layers. In the fissured granite layer, the aquifer compartment exploited with the A3 borehole is laterally limited by impervious boundaries, shaping the reservoir limits drawn on Figure 9 (Figure 12). The bottom of the model is impervious with a no-flow condition. However to allow the rise of deep mineralized water, a constant vertical flow of 8 m^3/h uniformly distributed over twenty cells is imposed. This upward flow is located in the area where a sub-vertical deep fault is expected from the hydrochemical spatial analysis (cf. § 3.4.1) and from the geological model. A uniform and constant recharge is imposed on the outcropping cells of the model, i.e. those of the Cenozoic formations located on the west of the fault separating Cenozoic formations from the granite, and those of the saprolite on the eastern part.

The permeability of the different layers of the model was set in agreement with the results of pumping test interpretations which notably highlighted that transmissivity values found for granite aquifer in the area are relatively high (i.e. about 10^{-3} m^2/s; hydraulic conductivity: $1.5x10^{-5}$ m/s) (Figure 8). The sub-vertical deep fault feeding the aquifer with deep mineralized fluid, which was not intercepted by any borehole, is defined as a more permeable zone than the surrounding layers with a vertical anisotropy (Kz = 10*Kxy).

3.5.2. Calibration and results

The hydrodynamic model calibration consisted in multiple steady state simulations with various parameters in order to fit at best piezometric levels and feature the observation data.

The recharge rate of the saprolite is the main calibrated parameter of the model. The applied recharge is 142.5 mm/year over the saprolite. A recharge rate of about 10% of this value is imposed (i.e. 15 mm/year) on the Cenozoic sedimentary deposits, which present a lower infiltration rate because of their low hydraulic conductivity. Other parameters as hydraulic conductivities of layers and location of boundaries are close to the ones defined by the analysis of pumping tests (i.e. hydraulic conductivity of post-rift sediments and saprolite 10^{-7}m/s and $5x10^{-9}$m/s respectively).

The extension and orientation of the sub-vertical fault in the granite and the value of the upflow of mineralized fluid were also adjusted during the calibration phase in order to match with the observed chemical contents at the various boreholes located within the A3 compartment.

In agreement with the main features of regional hydrogeology, the calibrated model in natural regime reveals generally east-west oriented flows, drained by the Coise stream. At the east of the boundary fault, groundwater from granitic layers overflows along the Coise stream and from two cells located on the right bank of the stream close to the historical Fontfort spring. In the central part of the A3 compartment along the Coise, the piezometric levels are less than 10 metres deep from the ground level. These elements are fully consistent with the description of the system at the beginning of the industrial abstraction as proposed by Archambault (1947). The sum of the overflow of the A3 reservoir on the right bank of the Coise is 15.3 m^3/h, i.e. 4.25 L/s, which seems to be a reasonable order of magnitude for this type of spring.

Under abstraction condition, the hydraulic heads are rather well reproduced (Table 1). The simulated hydrogeological system presents no overflow in the saprolite, which is consistent with current field observations. Outputs from the Cenozoic deposits to the Coise stream are less important (1.6 m^3/h) than in the natural state (4.6 m^3/h). Exchanges between the Cenozoic sediments and the unconsolidated saprolite are locally upwards, locally downwards, with a consistent spatial distribution, and are balanced on the entire modelled area. Considering only the A3 reservoir area, the Cenozoic aquifer feeds the unconsolidated saprolite (3.4 m^3/h), which had been previously highlighted by the interpretation of pumping tests (i.e. leakage effect).

Table 1: Comparison of modelled and measured hydraulic heads (metres above mean sea level) (steady state and under abstraction conditions) for A3 and observation boreholes in the A3 compartment. See location of the boreholes on Figure 9

	Modelled (m)	Measured (m)	Delta (m)
A3	307.88	307.2	+ 0.68
SG13	314.34	314.53	- 0.19
SG3bis	312.09	311.25	+ 0.84
Badoit IV	312.94	312.11	+ 0.83
Flute 70	311.37	311.64	- 0.27
A1	311.7	311.05	0.65
A2	310.43	310.48	- 0.05

3.5.3. Coupling with hydrochemical tool

After hydrodynamic calibration, the model was applied to validate and enhance with spatialized results the mixing model derived from the statistical analysis on the A3 groundwater. Indeed, the EMMA analysis showed that the water mineralization in the A3 compartment and the dynamic evolution of 6 major ions can be explained by a combination between two poles, one deep and mineralized, and a freshwater dilution pole. Steady state non reactive transport simulations were performed with the model in order to set boundary conditions regarding the location and composition of the inflows of water representative of these two poles. The final configuration allows simulating concentrations of major ions to be as close as possible to measured data in the boreholes (Figure 12). The deep pole is entering the system through the deep sub-vertical fault crossing the A3 compartment and the dilution pole is associated to the recharge over the outcropping saprolite to the east of the border fault. Figure 12 presents the simulated spatialized concentration of the Ca^{2+} ion which is well representative of the mixing rate between deep mineralized Ca^{2+} rich water and the dilution pole which is poorer in Ca^{2+}.

Table 2: Comparison of measured and modelled electrical conductivity and concentration of the main major ions (mg/L) in A3, SG3bis and SG13 boreholes from the A3 compartments (see Figure 9 for location of boreholes)

	µS/cm	*mg/l*							
	EC at 25°C	**SiO_2**	**Ca^{2+}**	**Mg^{2+}**	**Na^{+}**	**K^{+}**	**HCO_3^{-}**	**Cl^{-}**	**SO_4^{2-}**
A3 measured	1584	26	173	69	126	11	1115	71	54
A3 modelled	1451	23	162	61	104	10	938	66	53

Delta	***8.4%***	***9.8%***	***6.6%***	***12.1%***	***17.5%***	***9.2%***	***15.9%***	***7.6%***	***1.9%***
SG3Bis measured	1328	22	147	50	81	9	724	70	52
SG3bis modelled	1471	25	161	60	104	9	919	76	53
Delta	***-10.8%***	***-12.7%***	***-9.2%***	***-20.1%***	***-28.6%***	***-4.9%***	***-26.9%***	***-8.5%***	***-2.5%***
SG13 measured	508	16	53	20	36	4	223	43	32
SG13 modeled	426	13	30	6	40	10	105	36	22
Delta	***16.1%***	***18.1%***	***43.7%***	***71.7%***	***-12.3%***	***-161%***	***52.8%***	***16.4%***	***31.8%***

According to the proposed configuration of inflows into the system, the model water budget shows that 44% of recharge of the A3 compartment comes from the deep mineralized pole, 45% from the saprolite and 11% from leakage of Cenozoic formations. Sensitivity tests were carried out during the model construction and after the calibration phase to explore its capabilities. One will retain that: (i) the position and shape of the deep fault into the A3 compartment naturally affect results, especially on calculations of chemical concentration. An extension of the fault to the North is required to reproduce the high mineralization in SG3bis and the extension to the South-East to explain the lesser mineralization of SG13 (Figure 12); (ii) overall, a recharge on the Oligocene between 0 and 50 mm per year provides similar results.

The numerical model shows the consistency of all hydrodynamic and geochemical interpretations presented above and thus confirms the assumptions about the hydrogeochemical functioning of the A3 compartments. Also, it allowed the rather precise location of the deep fracture providing Ca-Mg-type deep mineralized water.

3.6. Hydrogeological conceptual model

The very good consistency between all the clues obtained from the various approaches implemented in the frame of this research (geological model, hydrodynamics, hydrogeochemistry, modelling, etc.) allows formulation of a realistic and robust hydrogeological conceptual model (Figs 13 and 14). Such a conceptual model is rather different from the ones already published for such CTMCG hydrosystems.

The Saint-Galmier's CTMCG aquifer is hosted within the stratiform fissured layer of the granite with a thickness of about 100-125 m, which lies below the low hydraulic conductivity of both Forez graben sediments and granite's saprolite. This stratiform fissured layer belongs to a weathering profile that developed during several phases of weathering. Indeed, the thin layer of unconsolidated saprolite and the unusual thickness of the laminated saprolite layer can be interpreted as resulting from a poly-phased weathering process (Dewandel et al., 2006). The abnormally thick laminated horizon surely developed on an ancient fissured layer inherited from a first weathering phase, re-weathered during a second weathering phase. There is no clear indication at Saint-Galmier about the age of these two phases, however, as known regionally (Lachassagne et al., 2015), the first one probably occurred during the Early Cretaceous and the second one during Early to Middle Eocene period, prior to Late Eocene to Oligocene graben filling. On the raised compartment of the graben (east part of the N-S regional fault), where the crystalline rocks now outcrops, the weathering processes are more or less continuous since the regional uprising during Late Miocene and erosion of Tertiary sedimentary deposits. Contrarily, weathering process on the granite below the graben's sediments surely stopped since Eocene.

The density of hydraulically conductive fractures of the stratiform fissured layer decreases with depth within the weathering profile, as classically observed in such profiles (see Dewandel et al., 2006 for instance). The fracture hydraulic conductivity of this aquifer appears to be mostly related to weathering processes; however tectonic structures or other discontinuities such as veins, joints, etc. (see Dewandel et al., 2011 or Lachassagne et al., 2011; Roques et al., 2016) may also contribute to the hydraulic conductivity of the aquifer. Compared to other data on hydrodynamical properties of such fissured layer in granite (Maréchal et al., 2004; Dewandel et al., 2006; 2011), the St-Galmier granite is characterized by high transmissivity values (between $8\,10^{-5}$ and 3.10^{-3} m^2/s in most

boreholes; Figure 8). These high values are believed to result from weathering processes, with a weathering-induced fissures density enhanced by the fracturing of the area. However, transmissivity of the fissured layer strongly decreases where it is buried below a high thickness of Oligocene sediments (down to 10^{-5} m^2/s). The origin of this decrease is yet to be investigated and understood: closing of the granite's subhorizontal fractures caused by the sedimentary deposits weight? Diagenetic clogging of the fractures?

As shown by boreholes and geophysics, this aquifer extends over a surface area of several square kilometres, which explains its overall long term productivity. It is however divided into several (at least 10), kilometre in length, hectometres in width, compartments. These compartments are all bounded by impervious boundaries. Most of these impervious boundaries -for instance for the Côte Rouge, Violes-Primevères, Aubignat, SB/SB', and quite surely for the Joyeuse-Frarie, Besacieux, Richelande and A3 compartments- are associated with a great confidence to identified faults. These faults all act as impervious boundaries either due to their impervious clayey fault gouge and/or as they offset the aquifer compartments one to the others and put in contact the aquifer with impervious layers such as, from bottom to top, the unfractured granite, the saprolite and the Oligocene sediments.

This aquifer is bounded at its bottom by the unfractured impervious granite, and at its top by the weathering profile's saprolite and, where present, by the Oligocene sedimentary cover, mostly also of very low hydraulic conductivity. The geological synthesis and modelling however allowed identifying two main lithological facies within the sediments: the clayey syn-rift sediments of very low hydraulic conductivity and the clayey-sandy post-rift sediments that locally exhibit higher hydraulic conductivities. The absence of the syn-rift sediments between the granite aquifer and the overlying post-rift sediments, but also locally the absence, due to erosion, of the saprolite, locally allows flow and/or leakage, and chiefly explains that in such specific areas the post-rift sediments are invaded by natural mineral water.

The aquifer is fed on the one hand by deep carbo-gaseous highly mineralized mineral water rising up only by a few permeable subvertical fractures or parts of fractures, and on the other hand by water from local aquifers recharged by rainfall. The latest are mostly granite aquifers slowly recharged as a consequence of the low hydraulic conductivity of the saprolite cover and Oligocene sediments. In the southern part of the CTMCG hydrosystem, it is a NW-SE subvertical fracture that feeds the A3, Pétillante and Généreuse compartments with carbogaseous Ca-Mg rich deep water. Nevertheless, the hydrogeological modelling of the A3 compartment showed that a short length of a N-S fracture, neighboring the NW-SE fracture, is also required. In the northern part of the CTMCG hydrosystem, only a segment of one N-S fracture is enough to explain the carbogaseous Na-rich pattern of water from the Violes-Primevères compartment. All the other compartments are interpreted to be either fed by waters arriving from other compartments (for instance "Joyeuse-Frarie" where a mixing between Ca-Mg and Na-rich waters occurs) or are not fed by deep mineral water (e.g. Côte Rouge and Aubignat) but only by the local recharge. The particularity of this case study is that the compartments are undergoing constant pumping. This provides an advantage for the interpretation because a flux toward the abstraction boreholes is created, and the pumped water is there representative of a larger area, which can overcome the low density of observations given the complexity of such a system (in average hardly a bit more of one borewell/piezometer per identified compartment). The study of geochemistry and piezometry allows validating the compartmentalization of the aquifer, as the chemical facies is different for each box and samples integrate the waters of each compartment by convergent fluxes. This hypothesis of flux converging towards abstraction boreholes within each compartment is largely supported by the few available piezometric data and the hydrochemistry.

Before the exploitation of the aquifer by pumping (till the XIX^{th} Century), the natural mineral water was naturally flowing out at the Fontfort spring which is the lowest place in the area, in the Coise stream valley, where the granite aquifer outcrops near the contact with the low permeability Oligocene sediments. The natural mineral water was also leaking upwards through the saprolite and/or the sedimentary cover, particularly in areas where the saprolite and/or the syn-rift low

permeability sediments were eroded. The exploitation of the aquifer by pumping modified the flux directions, and also mixings, in several compartments of the aquifer, particularly in the A3 and Joyeuse-Frarie compartments, and explains the current distribution of the natural mineral water hydrochemical facies in the aquifer.

4. Discussion

A realistic and robust hydrogeological conceptual model of a CTMCG hydrosystem is proposed based on a detailed characterization of the system: geology, hydrogeochemistry, hydrodynamic, modelling. In fact, to our opinion, only a multidisciplinary approach such as the one performed here (see also for instance Lachassagne et al., 2009; Maréchal et al., 2014) allows such an in-depth characterization for achieving a realistic conceptual model. It is the convergence of the clues obtained from the various methods, and not only clues of one method, that ensures the robustness of each part of the conceptual model and, overall, of the conceptual model globally.

This conceptual model is of course of great use for the day-to-day operational management of this NMW resource and its protection. It opens up further operational perspectives such as the numerical modelling of all the aquifer's compartments. However, the results of this research also open-up larger fundamental perspectives.

In such CTMCG hydrosystems, "the aquifer" at the origin of the carbogaseous natural mineral water is rarely identified, and most authors vaguely consider that, as the hydrosystem is fractured, the tectonic fractures that provide the deep groundwater also constitute "the main or the only possible aquifer" (e.g. Stober and Bucher 1999). For St-Galmier CTMCG, we clearly demonstrate that:

(i) the fissured stratiform layer of the crystalline rock's (here a granite) weathering profile constitutes "the aquifer". This large and thick aquifer explains the high hydrogeological inertia of the studied boreholes and can be numerically modelled similarly to a porous aquifer (see also Lachassagne et al., 2001);

(ii) as a consequence, this aquifer has a large extension (several square kilometres) and is "easily" reached by any vertical borehole, which explains the quite high quantitative success of the drillings in this area, as compared for instance to other CTMCG aquifers where this weathering profile was totally eroded (see for instance the case study of Vals-les-Bains, France; Ledoux et al., 2016);

(iii) this aquifer is compartmented by faults that all act as impervious boundaries. The low hydraulic conductivity of most faults was already largely demonstrated (see the references cited in the Introduction). However, it does not prevent to continue to advertise about this fact as several hydrogeologists "naturally" tend to consider the contrary;

(iv) this aquifer is only very locally fed by deep highly mineralized carbo-gaseous water originating from a few segments of subvertical tectonic fractures that only constitute a few percents of the total length of identified faults.

This duality (fractures locally pervious but mostly impervious) has been previously mentioned (e.g. Bense et al. 2013). More recently, in the same structural context (i.e. peri-Alpine graben), Gumm et al. (2016) highlighted the rise of deep fluid along faults that also act as barrier for the shallow compartments. Of course, some tectonic fractures may locally "boost" the hydraulic conductivity of the aquifer. It will be one of the future challenges of research on this site to try to identify if such areas exist, to find a mean to distinguish both types of fracturing (weathering and tectonic respectively) and their associated hydrodynamic properties.

As a research perspective and with the objective to generalize the concepts developed in this paper, particularly the one from § (ii) above, it would also be of high interest to re-examine, on the one hand the data from CTMCG located in a similar context where the weathering profile may have been preserved from erosion (for instance the CTMCG bordering grabens filled with sediments, see for instance Figure 1), and, on the other hand, CTMCG where the weathering profile was eroded, to deepen the interpretation presented in this paper. Moreover, this re-analysis may help to better understand their geological structure and hydrogeological functioning and further to help their management and protection.

Moreover, the approach presented in this paper also allowed the precise location and the characterization (orientation, hydrochemistry of the deep water produced by the fracture) of some, or quite surely all, of the subvertical tectonic fractures feeding the aquifer with deep highly mineralized carbo-gaseous water. In other studies, such a trial to characterize these fractures is often only resulting from a geological structural analysis or, worse, only by a "lineament study", without any strong and robust demonstration. We here also consider that such a multidisciplinary approach comprising, among others (of course a strong structural and geological model), a hydrodynamic and hydrochemical approach (synthesized, in the A3 well compartment, by the numerical modelling) is much more robust to identify and characterize such feeding fractures. In a previous similar study (Maréchal et al., 2014), we showed that such fractures weren't detected at all by the only classical geological and structural approach.

Analysis of the spatial distribution of mineralization of groundwater shows that the deep fractures play a major role on the facies of mineral waters. The gas enriched waters rise up under hydraulic and thermal gradient effect thanks to some segments of the sub-vertical faults. They drain deep fluids and mantellic CO_2 (Blavoux, 1993). However, mineral waters have variable chemical facies and appear either Ca-Mg-type (typical Saint-Galmier facies) or Na-type. To date, the most reasonable explanation for the variability of the chemical facies is that uprising fluids are enriched in various cations according to the nature of the granite and the encountered secondary minerals within the faults throughout the ascent of the fluid.

5. Conclusion

This multidisciplinary study (geology, hydrogeology, geochemistry and modelling) has clarified the hydrogeological functioning of the Saint-Galmier carbo-gaseous system thanks to the confrontation using results from complementary methods.

The geological approach was based upon numerous available data (logs drilling, seismic, gravimetric and field surveys) and allowed the realization of a 3D geological and structural model. Then, on the basis of this geological model and, hydrodynamic and geochemical data, a robust and realistic conceptual hydrogeological model was built. It highlights the high compartmentalization of the aquifer system and the mixing between deep mineralized water ascending through deep faults and more superficial dilution pole within each compartment.

The permeability of the crystalline aquifer is found to be relatively high, especially when the sedimentary cover is thin. The fissured layer of the weathering profile plays a major hydrodynamic role compared to tectonic faults as it hosts thick and extended aquifers, delimited by low hydraulic conductivity faults.

A deterministic hydrogeological model of the A3 compartment has been implemented with the aim to validate the functioning hypotheses that emerged from these complementary approaches. The hypotheses were tested successfully and the numerical model proposes a very sound solution for the orientation and the location of the fault segments providing deep mineral fluids. The comparison of the information from the transport simulations with data from geochemical analysis (EMMA) makes possible the estimation of the signature of the Ca-Mg-type mineralized pole of this major reservoir.

The chemical variability of the mineralized water in such a restricted area is, to date, explained by the probable variability of the hydrothermally dissolved minerals, but we are not able to clearly state on the origin of the very localized Saint-Galmier facies (i.e. Ca-Mg type carbo-gaseous mineral water). The original composition of the deep mineralized poles and the associated mineralization processes, the transit time and mixing rates within the compartments still remains largely unknown. With this goal in mind, additional sampling were run in 2015 for a wide range of tracers analyses (e.g. major ions, stable isotopes of the water molecule, $\delta^{13}C$, $^{87}Sr/^{86}Sr$, $^{234}U/^{238}U$, ^{226}Ra, ^{222}Rn, noble gases, $^{3}He/^{4}He$, SF6, ^{3}H, ^{39}Ar and ^{85}Kr) and should provide additional information.

Acknowledgements

This study was conducted under a research agreement between Evian Volvic World (Danone Waters France) and BRGM. The authors are grateful to the two reviewers and the editor for their fruitful comments, remarks and proposals that helped improving the manuscript.

References

Acworth R. I. 1987. The development of crystalline basement aquifers in a tropical environment. Q. J. Eng. Geol. Hydrogeol. 20(4), 265-272

Archambault J. 1947. Etude hydrogéologique du gisement d'eaux minérales de Saint Galmier (Loire)

Barbarin B., Gerbe M.-C., Vitel G., Gonord H., Couette F. 2012a. Carte géologique France (1/50 000), feuille Firminy (744). Orléans, BRGM

Barbarin B., Gonord H., Vitel G., Couette F., Gerbe M.-C., Becq-Giraudon J.-F., Lagarigue J.-L. 2012b. Notice explicative, Carte géologique France (1/50 000), feuille Firminy (744). Orléans, BRGM, 129 p

Barnes I., Irwin W. P., & White D. E. 1984. Map showing world distribution of carbon-dioxide springs and major zones of seismicity. US Geological Survey

Blavoux, B. 1993. Le gisement de l'eau minérale Badoit – Structure géologique, hydrogéologie et géochimie, définition et fonctionnement du système minéral, caractéristiques du mélange Badoit et de ces composantes, Université d'Avignon, 52 p

Bense V.F., Gleeson T., Loveless S.E., Bour O., Scibek J. 2013. Fault zone hydrogeology. Earth-Sci. Rev. 127, 171–192

Bourdet D., Ayoud J.A. and Prirard Y.M. 1989. Use of pressure derivative in well-test interpretation. SPE, 293-302

Bourdet, Whittle T.M., Dougals A.A., Pirard V.M. 1983. A new set of type curves simplifies well test analysis, World Oil

Briot D., Poidevin J.-L., Leyrit H., Gonord H., Gerbe M.-C. 2001. Les fossés d'effondrement tertiaires. In « La géologie du Massif Central », Géologues 130/131, 59-65

Burns D. A., McDonnell J. J., Hooper R. P., Peters N. E., Freer J. E., Kendall C., & Beven K. 2001. Quantifying contributions to storm runoff through end-member mixing analysis and hydrologic measurements at the Panola Mountain Research Watershed (Georgia, USA). Hydrol. Process. 15(10), 1903-1924

Calcagno P., Chiles J.P., Courrioux G., Guillen A. 2008. Geological modelling from field data and geological knowledge; Part I, Modelling method coupling 3D potential-field interpolation and geological rules. Phys. Earth Planet. Inter. 171 (1-4), 147-157

Calcagno P., Courrioux G., Guille A., Fitzgerald D., Mcinerney P. 2006. How 3D implicit Geometric Modelling Helps To Understand Geology: The 3DGeoModeller Methodology. Int. Assoc. for Mathematical Geology. XIth International Congress, Université de Liège – Belgium. Liège – September, 3rd - 8th 2006 S14-06

CGG, 1990. Rapport de mise en oeuvre et d'interprétation de sismique réflexion haute résolution, Compagnie Générale de Géophysique, mission 100.25.43. 16 p

Chilton P. J., & Foster S. S. D. 1995. Hydrogeological characterisation and water-supply potential of basement aquifers in tropical Africa. Hydrogeol. J. 3(1), 36-49

Christophersen N. and Hooper R. P. 1992. Multivariate analysis of stream water chemical data: The use of principal components analysis for the end-member mixing problem. Water Resour. Res. 28(1), 99-107

Cinti D., Tassi F., Procesi M., Bonini M., Capecchiacci F., Voltattorni N., … Quattrocchi F. 2014. Fluid geochemistry and geothermometry in the unexploited geothermal field of the Vicano–Cimino Volcanic District (Central Italy). Chem. Geol. 371, 96–114

Couëffé R., Grataloup S., Wyns R, et B. Dewandel. 2014. Système minéral carbo-gazeux de SAINT-GALMIER (Saint-Galmier - Loire): Révision des données géologiques et réalisation d'un modèle géologique 3D. Rapport BRGM/RC-64214-FR

Courrioux G., Aug C., Bourgine B., Chilès J-P. 2006. Integration of inequality constraints on the location of geological interfaces in 3D geological modeling. Int. Assoc. for Mathematical Geology. XIth International Congress, Université de Liège – Belgium. Liège – September, 3rd - 8th 2006 S14-10

748 Courtois N., Lachassagne P., Wyns R., Blanchin R., Bougaïre F.D., Somé S., Tapsoba A. 2010. Large
749 scale mapping of hard rock aquifer properties applied to Burkina Faso, Ground Water 48(2),
750 269-283
751 Deruyck B., Ehlig-Economides C., & Joseph J. 1992. Testing design and analysis. Oilfield Review 4(2),
752 28-45
753 Dewandel B., Lachassagne P., Boudier F., Al Hattali S., Ladouche B., Pinault J.L. and Al-Suleimani Z.
754 2005. A conceptual model of the structure and functioning of the Oman ophiolite hard-rock
755 aquifer through a pluridisciplinary and multiscale approach. Hydrogeol. J. 13, 708-726
756 Dewandel B., Lachassagne P., Wyns R., Maréchal J. C., & Krishnamurthy N. S. 2006. A generalized 3-D
757 geological and hydrogeological conceptual model of granite aquifers controlled by single or
758 multiphase weathering. J. Hydrol. 330(1), 260-284
759 Dewandel B., Lachassagne P., Zaidi F. K., & Chandra S. 2011. A conceptual hydrodynamic model of a
760 geological discontinuity in hard rock aquifers: Example of a quartz reef in granitic terrain in
761 South India. J. Hydrol. 405(3), 474-487
762 Dewandel B., Aunay B., Maréchal J.C., Roques C., Bour O., Mougin B., Aquilina L. 2014. Analytical
763 solutions for analysing pumping tests in a sub-vertical and anisotropic fault zone draining
764 shallow aquifers. J. Hydrol. 509, 115–131
765 Duboeuf P., Eberentz P. Bligny J.-C. 1991. Prospection sismique sur le site de Saint-Galmier (42).
766 Synthèse des résultats. Rapport BRGM/R33775, 14 p
767 Duclos P. 1967. Géologie et minéralisations uranifères de la plaine tertiaire du Forez (Massif Central
768 Français). Thèse de doctorat, Université de Clermont-Ferrand, 104 p
769 Duclos P., Lorenchet de Montjamont M., Dheler R., Hernandez J., Peter-Longo J.M. 1974. Carte
770 géologique de la France à 1/50 000 – Feuille n°720 – Montbrison. BRGM ed., Orléans, France
771 Ech-Cherif El Khettani D., 1996. Géologie du fossé du Forez: essai de synthèse et comparaisons avec
772 les autres bassins tertiaires du Massif central français. Thèse de Doctorat, Université J.
773 Monnet, Saint-Etienne, 372 p
774 Ehlig-Economides C.A., 1988. Use of the pressure derivative for diagnosing pressure-transient
775 behavior. J. Petrol. Technol. (October), 1280–1288
776 Feybesse J.L., Lardeaux J.M.,Tegyey M., Gardien V., Peter-Longo J.M., Kerrien Y., Becq-Giraudon J.F.
777 1996. Carte géologique de la France (1/50 000) – Feuille n°721 - Saint-Symphorien-sur-Coise.
778 BRGM ed., Orléans, France
779 Forster C., Smith L. 1989. The influence of groundwater flow on thermal regimes in mountainous
780 terrain: A model study. J. Geophys. Res. Solid Earth, 94(B7), 9439-9451
781 Gerbe M.-C., Gonord H., Arnaud N. 1998. Age miocène des formations de bordure du fossé du Forez
782 (Massif central). Géologie de la France, 2, 47-53
783 Gumm L.P., Bense V.F., Dennis P.F., Hiscock K.M., Cremer N., Simon S. 2016. Dissolved noble gases
784 and stable isotopes as tracers of preferential fluid flow along faults in the Lower Rhine
785 Embayment, Germany. Hydrogeol. J. 24(1), 99-108. DOI: 10.1007/s10040-015-1321-7
786 Hantush, M.S. 1961. Aquifer tests on partially penetrating wells. J. Hydrau. Div., Proc. of the Am. Soc.
787 of Civil Engineers, 87, 171-195
788 Hunt B. and Scott D. 2007. Flow to well in a two-aquifer system. J. Hydrol. Eng. 12(2), 146-155
789 Kerrick D. M., McKibben M. A., Seward T. M., & Caldeira K. 1995. Convective hydrothermal CO2
790 emission from high heat flow regions. Chem. Geol., 121(1), 285–293
791 Lachassagne P., Golaz C., Maréchal J.C., Thiery D., Touchard F., Wyns R. 2001. A methodology for the
792 mathematical modelling of hard-rock aquifers at catchment scale, based on the geological
793 structure and the hydrogeological functioning of the aquifer. XXXI IAH Congress, Munich, in: K.-
794 P. Seiler and S. Wohnlich (Ed.), New approaches characterising groundwater flow, AA Balkema
795 Publishers, 367-370Lachassagne P., Maréchal J.C., Sanjuan B. 2009. Hydrogeological model of a
796 high energy geothermal field (Bouillante area, Guadeloupe, French West Indies). Hydrogeol. J.,
797 17, 1589–1606
798 Lachassagne P., Wyns, R., Dewandel B. 2011. The fracture permeability of hard rocks aquifers is due
799 neither to tectonics, nor to unloading, but to weathering processes. Terra Nova, 23, 145-161

Lajaunie C., Courrioux G., Manuel L. 1997. Foliation fields and 3D cartography in geology: principles of a method based on potential interpolation. Math. Geol. 29, 571-584

Lachassagne P., Maréchal J. C., Bienfait P., Lacquement F., & Lamotte C. 2015. Computing the Water Inflows Discharge and Assessing the Impacts of Tunnels Drilled in Hard Rocks: The A89 (France) Motorway Case Study. In Engineering Geology for Society and Territory, 3, 595-599. Springer International Publishing

Ledoux E., Xiao H., Terrisse J.F., Lachassagne P. 2016. Chapter 3.2 - Deterministic modelling of the Vals-les-bains carbo-gaseous natural mineral hydrosystem and analysis of sensitivity to changes in land use and water management practices. In “Forest and the Water Cycle: Quantity, Quality, Management". Lachassagne P., Lafforgue M., Eds., Cambridge Scholars Publishing, 266-291

Le Griel A. 1984. Géologie et relief de la Plaine du Forez. Paysages et milieux naturels de la plaine du Forez. CEF, Université de Saint-Etienne, 139-188

Lopoukhine M. 1998. Le patrimoine français des sources d’eau minérale. Réalités industrielles (MAI), 13-19

Maréchal J.C., B. Dewandel, K. Subrahmanyan. 2004. Contribution of hydraulic tests at different scale to the characterisation of fracture network properties in hard-rock aquifers. Water Resour. Res. 40 (W11508), 1-17Maréchal J. C., Lachassagne P., Ladouche B., Dewandel B., Lanini S., Le Strat P., & Petelet-Giraud E. 2014. Structure and hydrogeochemical functioning of a sparkling natural mineral water system determined using a multidisciplinary approach: a case study from southern France. Hydrogeol. J. 22(1), 47–68

Matthews A., Fouillac C., Hill R., O’Nions R. K., & Oxburgh, E. R. 1987. Mantle-derived volatiles in continental crust: the Massif Central of France. Earth Planet. Sci. Lett. 85(1–3), 117–128

Mohamed EA, Worden RH. 2006. Groundwater compartmentalization: a water table height and geochemical analysis of the structural controls on the subdivision of a major aquifer, the Sherwood Sandstone, Merseyside, UK. Hydrol. Earth Syst. Sc., 10, 49–64

Petrella E., Aquino D., Fiorillo F., Celico F. 2015. The effect of low-permeability fault zones on groundwater flow in a compartmentalized system. Experimental evidence from a carbonate aquifer (Southern Italy). Hydrol. Process. 29(6), 1577-1587

Renac C., Gal F., Ménot R.-P., Squarcioni P., & Perrache C. 2009. Mean recharge times and chemical modelling transfers from shallow groundwater to mineralized thermal waters at Montrond-les-Bains, Eastern Massif Central, France. J. Hydrol. 376(1), 1–15

Renard P. 2005. The future of hydraulic tests. Hydrogeol. J. 13, 259–262

Renard P., Glenz D. and M. Mejias. 2009. Understanding diagnostic plots for well-test interpretation. Hydrogeol. J. 17, 589–600

Roques C., Bour O., Aquilina L., Dewandel B., Leray S. et al. 2014. Hydrological behavior of a deep sub-vertical fault in crystalline basement and relationships with surrounding reservoirs. J. Hydrol. 504, 42-54

Roques C., Bour O., Aquilina L., Dewandel B. 2016-in press. High-yielding aquifers in crystalline basement: insights about the role of fault zones. Accepted in Hydrogeol. J.

Spane F.A. and Wurstner S.K. 1993. DERIV: a computer program for calculating pressures derivatives fir use in hydraulic test analysis

Stober I., Bucher K. (1999). Deep groundwater in the crystalline basement of the Black Forest region. Appl. geochem. 14(2), 237-254

Thiéry D. 1990. Software MARTHE. Modelling of Aquifers with Rectangular grid in Transient state for Hydrodynamic calculations of hEads and flows. Release 4.3. Rap. BRGM 4S/EAU n°R32548.

Thiéry D. 2010. Groudwater Flow Modeling in Porous Media Using MARTHE. In “Modeling Software Volume 5, Chapter 4, 45-60. Environmental Hydraulics Series”. Tanguy J.M. (Ed.) – Editions Wiley/ISTE London. ISBN: 978-1-8421-157-5

Tokan-Lawal, A., Prodanović, M., Eichhubl, P. 2015. Investigating flow properties of partially cemented fractures in Travis Peak Formation using image-based pore-scale modeling. Journal of Geophysical Research: Solid Earth 120(8), 5453-5466

852 Weinlich, F. H. 2005. Isotopically light carbon dioxide in nitrogen rich gases: the gas distribution
853 pattern in the French Massif Central, the Eifel and the western Eger Rift. Ann. Geophys, 48(1),
854 19-31
855 Wyns R., Baltassat J.M., Lachassagne P., Legchenko A., Vairon J. and Mathieu F., 2004. Application of
856 SNMR soundings for groundwater reserves mapping in weathered basement rocks (Brittany,
857 France), Bull. Soc. Géol. France, 175 (1), 21-34.

Figures

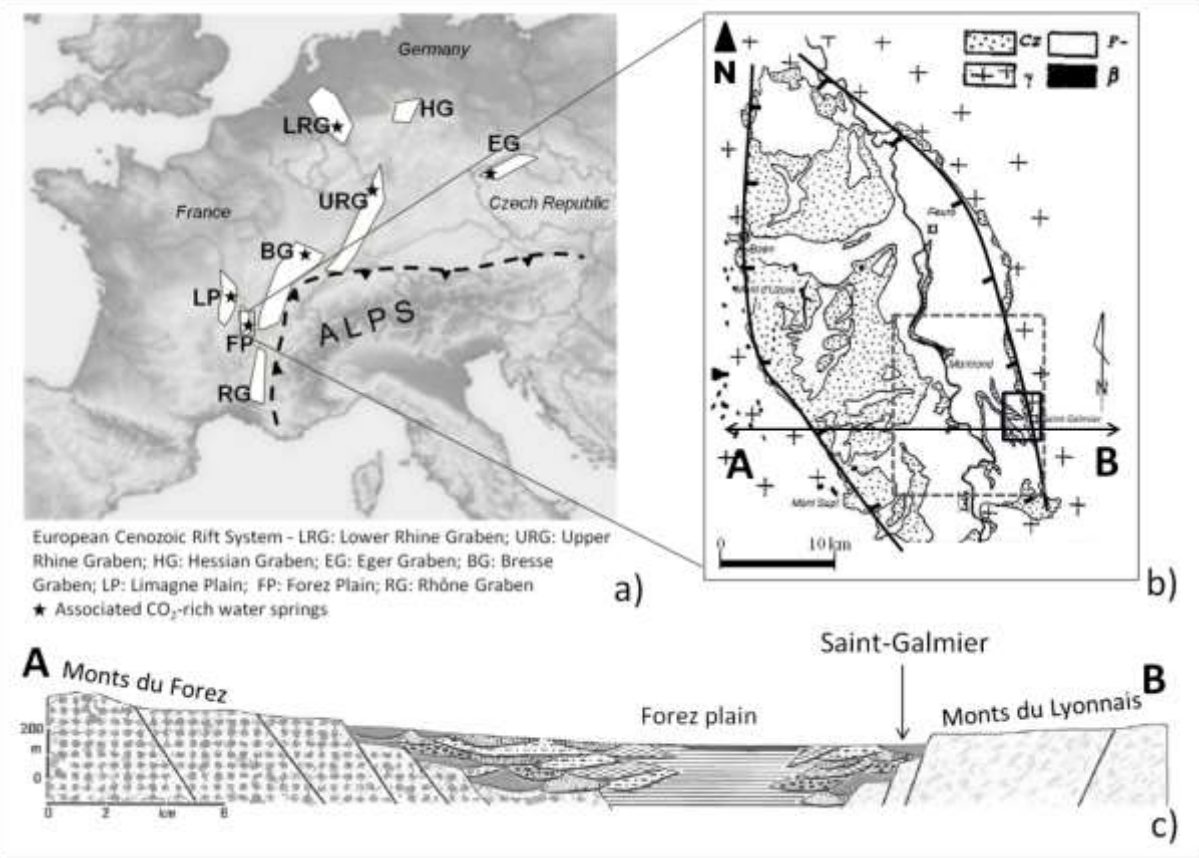

Figure 1: a) Location of the main peri-alpine grabens of the European Cenozoic Graben System; b) Main geological outcrops of the Forez Graben delimited by the main regional normal faults, cz: Cenozoic sedimentary deposits; F: Quaternary alluvium and colluvium; γ: Paleozoic bedrock; β Miocene volcanic formations (blue frame: geological model extended area and red frame: narrow geological model area) (Gerbe et al., 1998 modified); c) Schematic profile of the Forez Graben along the AB section. From West to East: the Monts du Forez massif (granite), the Forez plain (heterogeneous continental deposits) and the Monts du Lyonnais massif (metamorphic bedrock intruded by the granitic pluton of Saint-Galmier) (adapted from Le Griel, 1984).

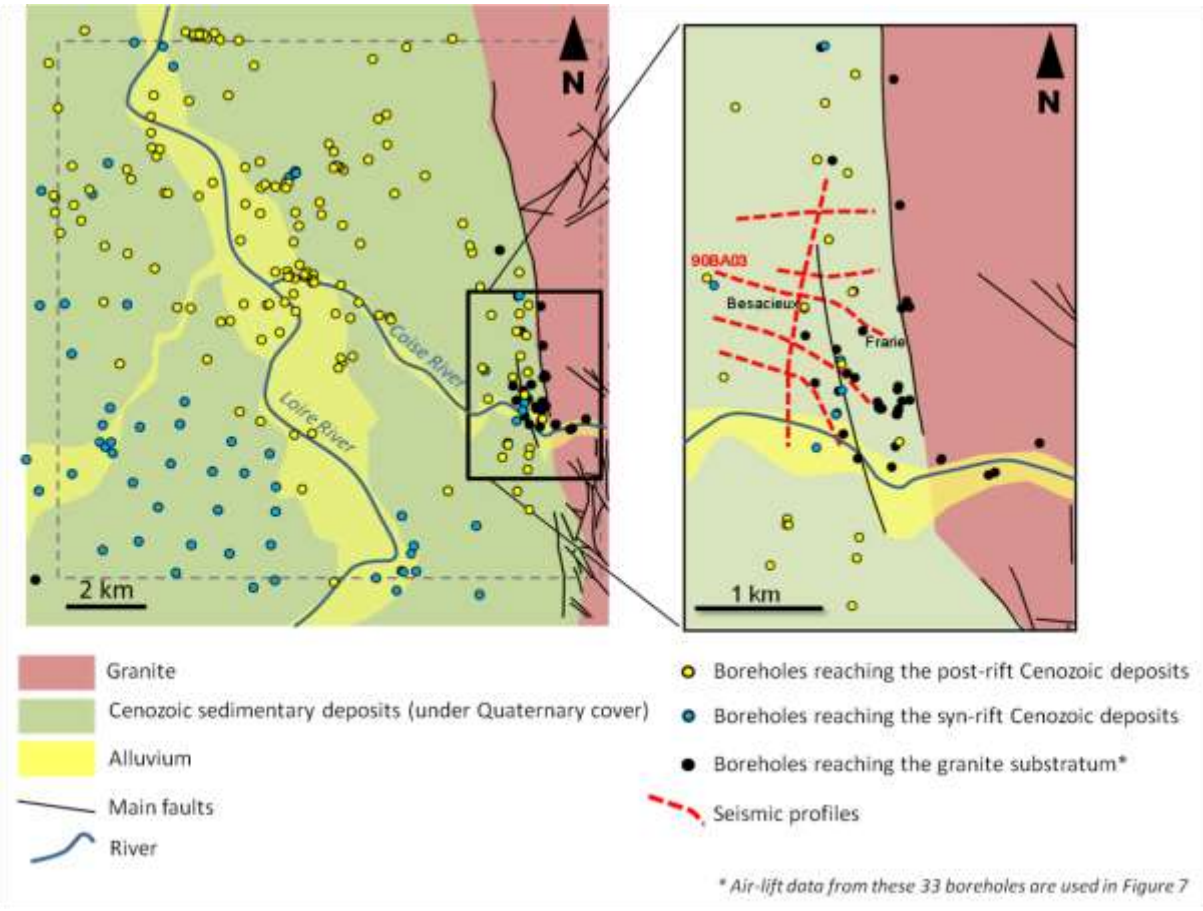

Figure 2: Location of boreholes and seismic profiles. The extended geological model area is contoured in dashed line and the narrow geological model area is contoured in continuous line. Simplified geology and faults from the 1/50.000 BRGM geological map (Feybesse et al., 1996). 90BA03 seismic profile interpreted in the Figure 3, Besacieux and Frarie boreholes are identified.

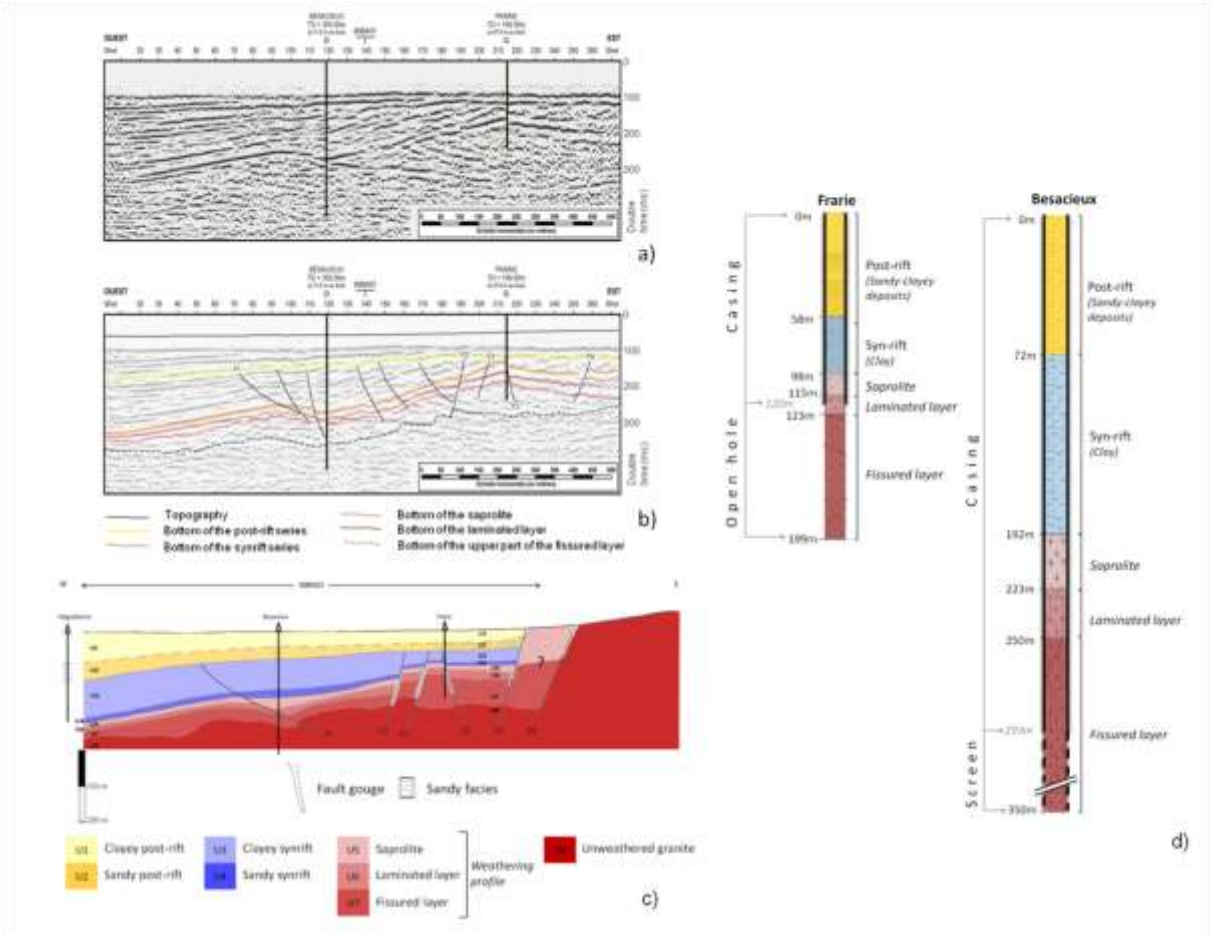

Figure 3: a) Digitized raw data of the 90BA03 seismic profile (see location on Figure 2); b) Line drawing (note the sealing of syn-rift normal faults by post-rift deposits); c) Geological cross section obtained by conversion from seismic times to depths and complementary borehole data d) Simplified technical and geological logs of Besacieux and Frarie boreholes.

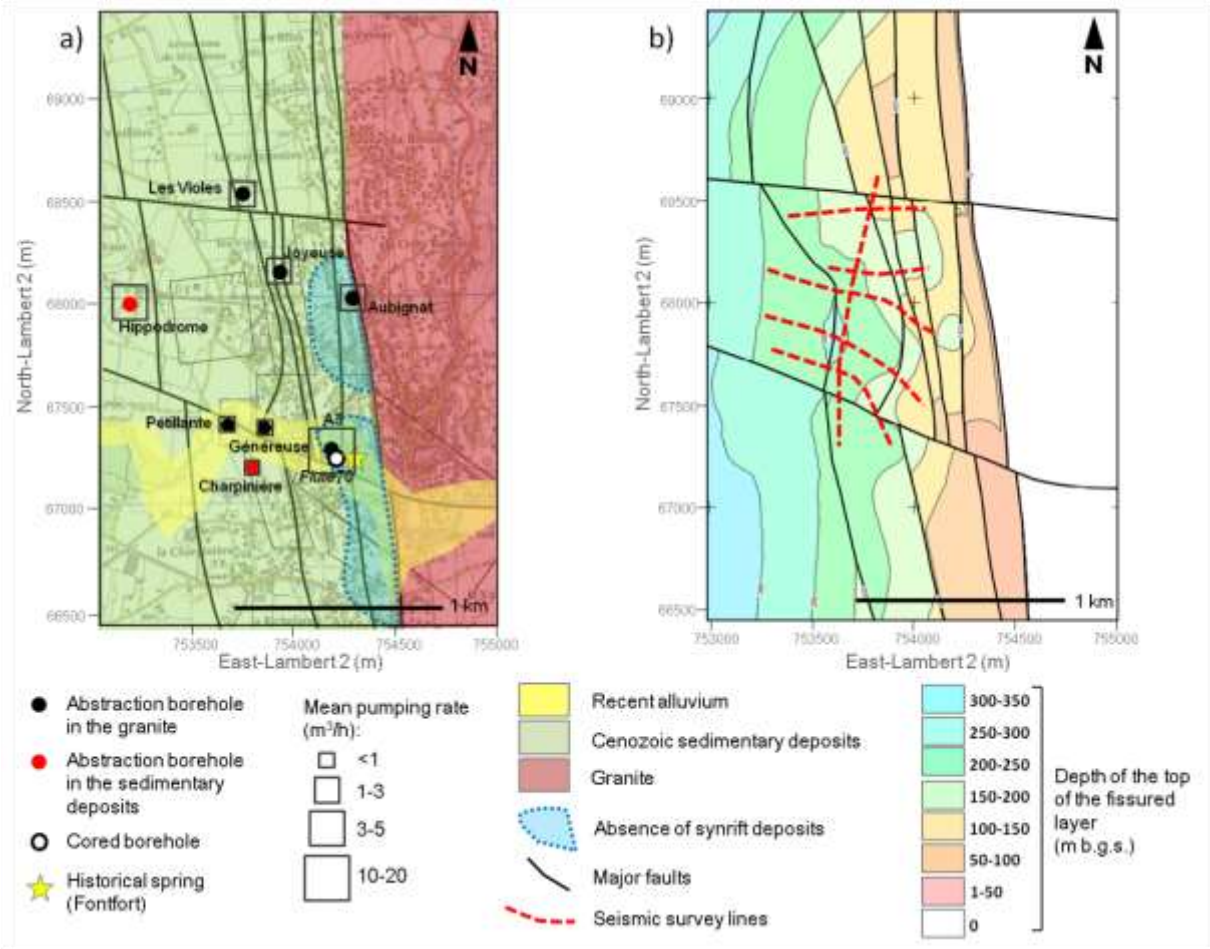

Figure 4: a) Simplified geological and structural sketch of the narrow area deduced from the 3-D geological model. Location of the abstraction boreholes within the area and their mean pumping rates. Location of the historical spring (Fontfort) and the cored borehole (Flute 70); b) depth of the top of the granite' fissured layer and structural sketch. Location of the seismic survey lines. Scale in meters (Lambert 2 coordinate system).

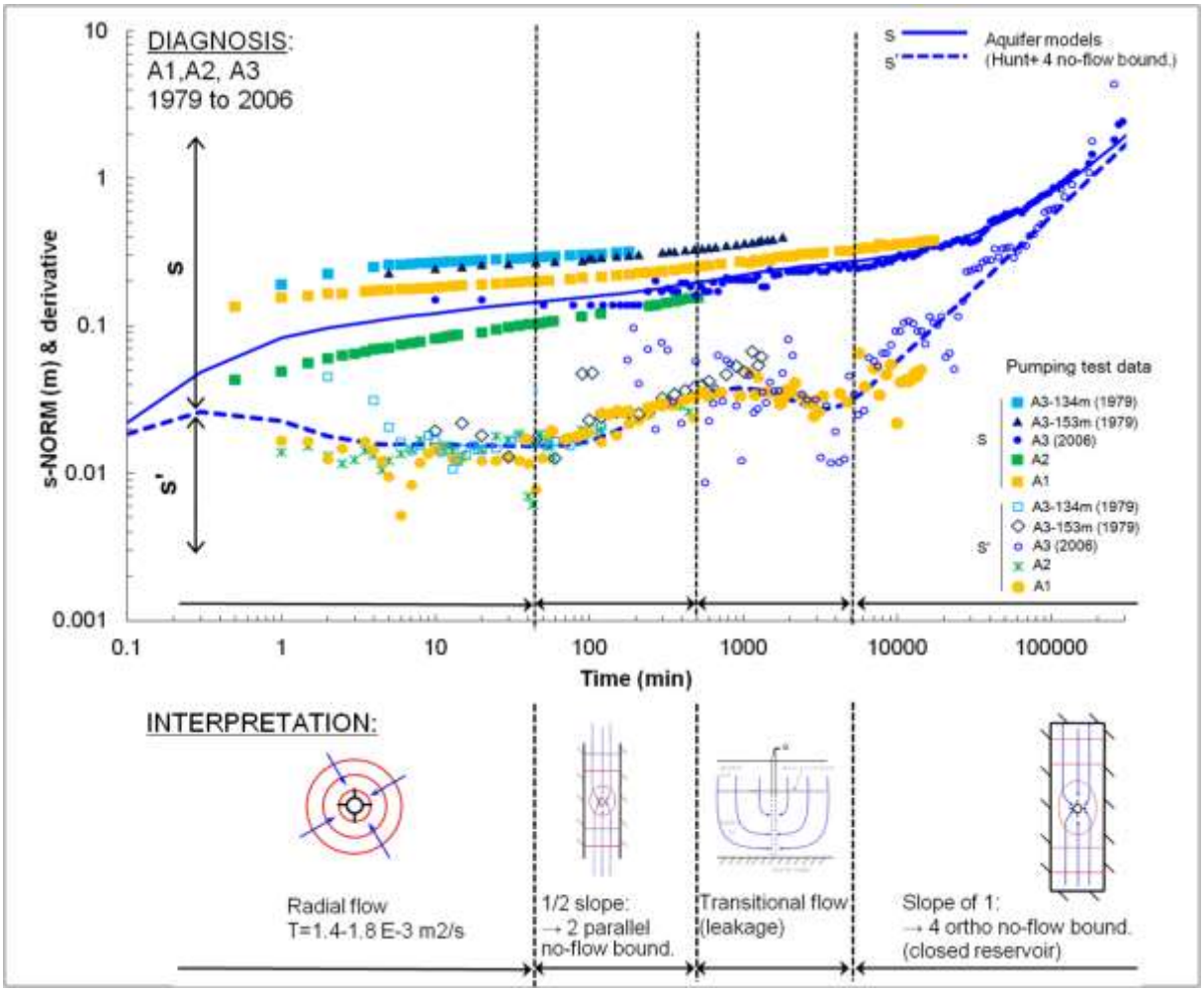

Figure 5: Example of pumping test interpretation in granite. Diagnosis and modelling of the tests performed in A1 (1 test), A2 (1 test) and A3 (2 tests at variable depth, 134 and 153 m; and 1 long duration test in 2006)) from 1979 to 2006. Model (A3-2006 only): Hunt and Scott (2007) and 4 no-flow boundaries and well effects.

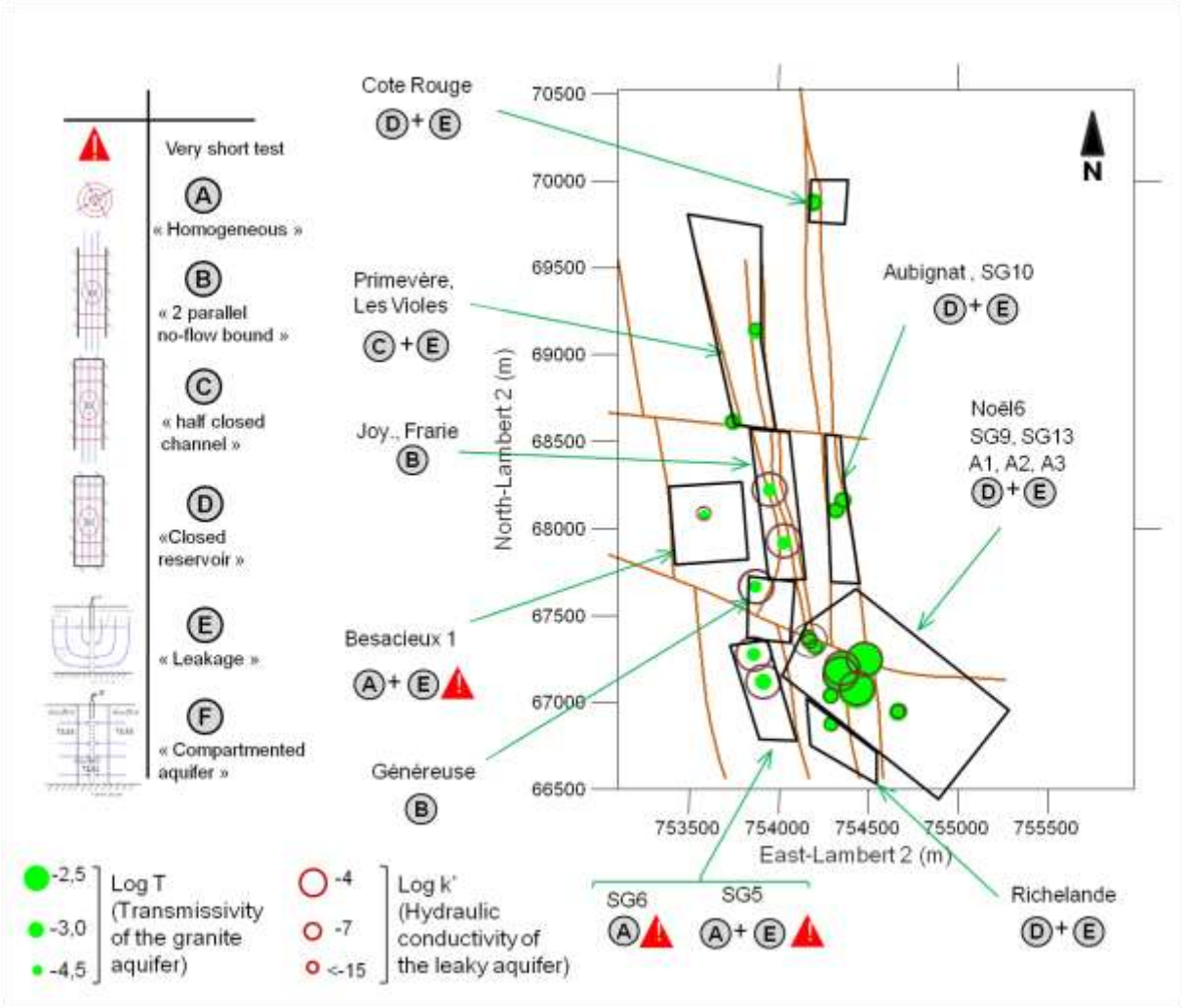

887

888 Figure 6: Synthesis of pumping tests interpretation in the granite aquifer: Transmissivity (T) of the
889 granite aquifer and hydraulic conductivity (K') of the leaky aquifer values ($Log_{10}T$ scale). Diagnosis for
890 each borehole (A to F), and identification of theoretical aquifer compartments limited by impervious
891 boundaries (black boxes). Scale in meters (Lambert 2 coordinate system).

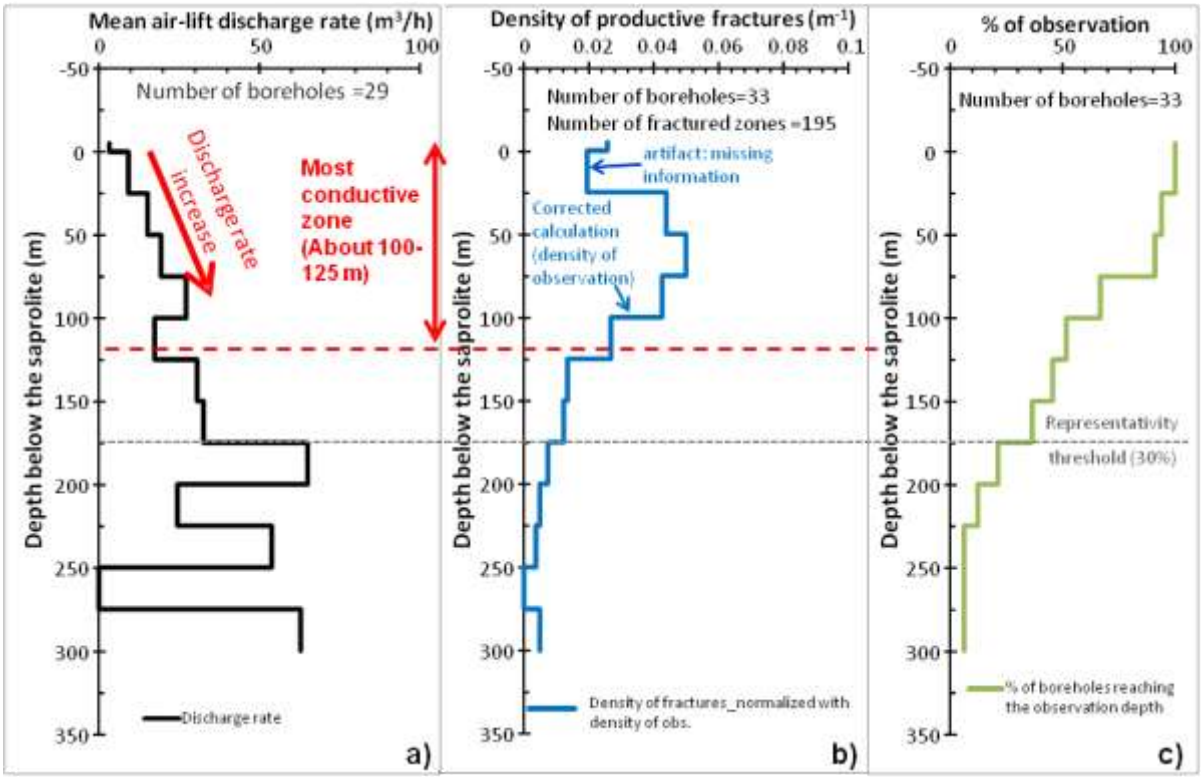

Figure 7: Air-lift analysis results for all the boreholes located into the granite aquifers (See Figure 2 for the location of boreholes). The discharge rates are represented as a function of the depth below the bottom of the saprolite. Part c) allows to define the representativeness of the analysis (density of observation in % of the number of boreholes vs. depth). Parts a) and b) allow identifying the most permeable area. a) mean discharge rate, b) corrected fracture density (according to the density of observation, see explanation in the text). NB: these graphs are significant for at least a density of observation of 30%, i.e. until a 150-175 m depth under the bottom of the saprolite.

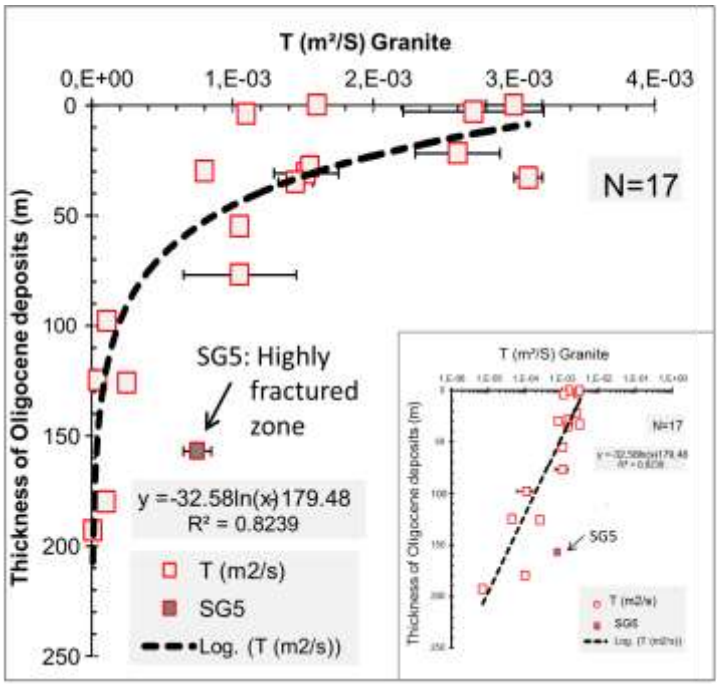

Figure 8: Estimated transmissivity of the granite aquifer vs. thickness of the Cenozoic sedimentary deposits (Log scale representation for horizontal axis (T) in the lower right corner; N= 17, SG5 data not comprised). The granite's transmissivity decreases as a function of the sedimentary cover thickness.

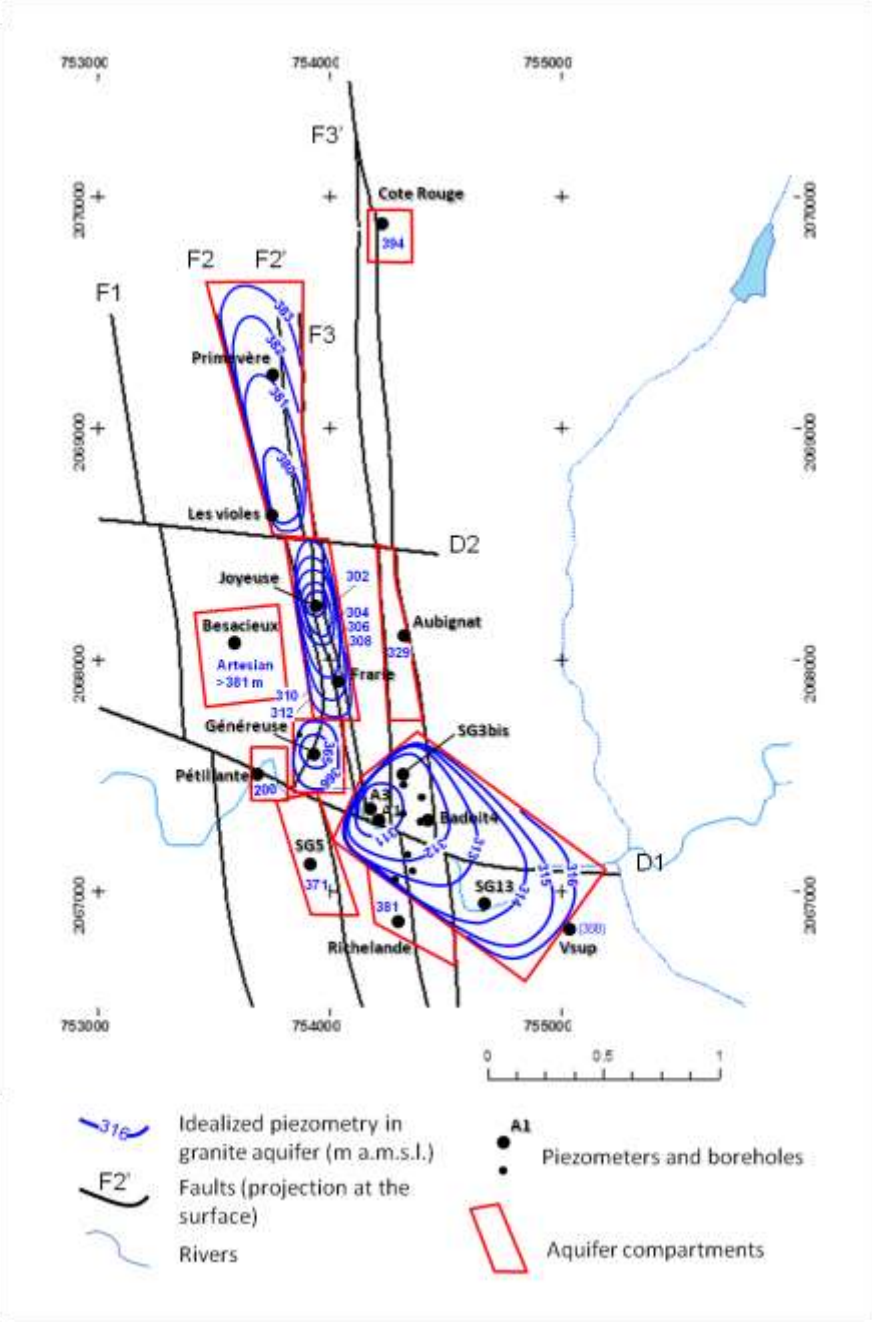

907

908 Figure 9: Location and delineation of the main granite aquifers on the basis of the geological and structural
909 modelling, and the interpretation of pumping tests and air-lift data. Main faults are projected on the surface
910 and represented in black lines. Aquifer compartments deduced from the hydrodynamic study in the main
911 boreholes are represented in red. The piezometric scheme is figured (in blue) in each compartment.

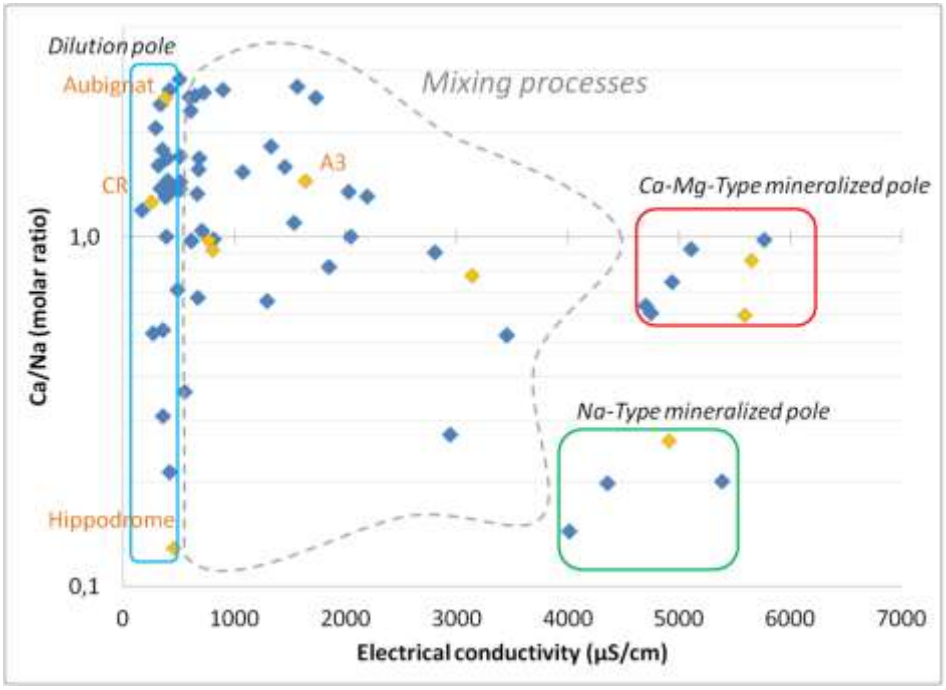

912

913 Figure 10: Molar Ca/Na ratio vs. electrical conductivity of groundwater of the Saint-Galmier aquifer system. Ca-
914 Mg-type and Na-type deep mineralized poles, dilutive pole and mixing processes are identified. Exploitation
915 boreholes are represented in orange.

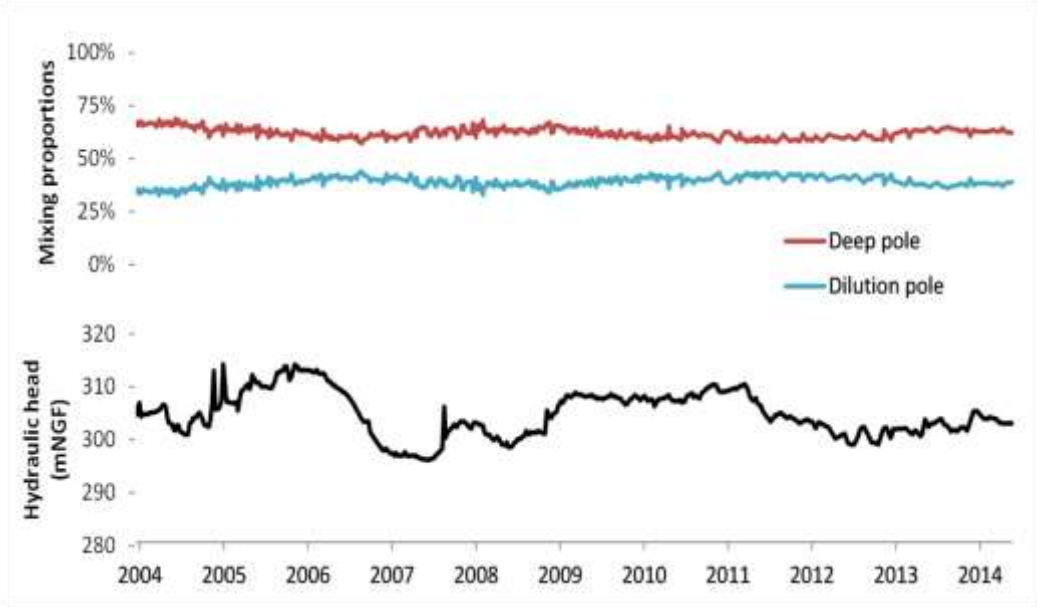

916

917 Figure 11: Time series of the mixing proportions of the deep pole and the dilution pole, and corresponding
918 hydraulic head of A3 borehole over the 2004-2014 period.

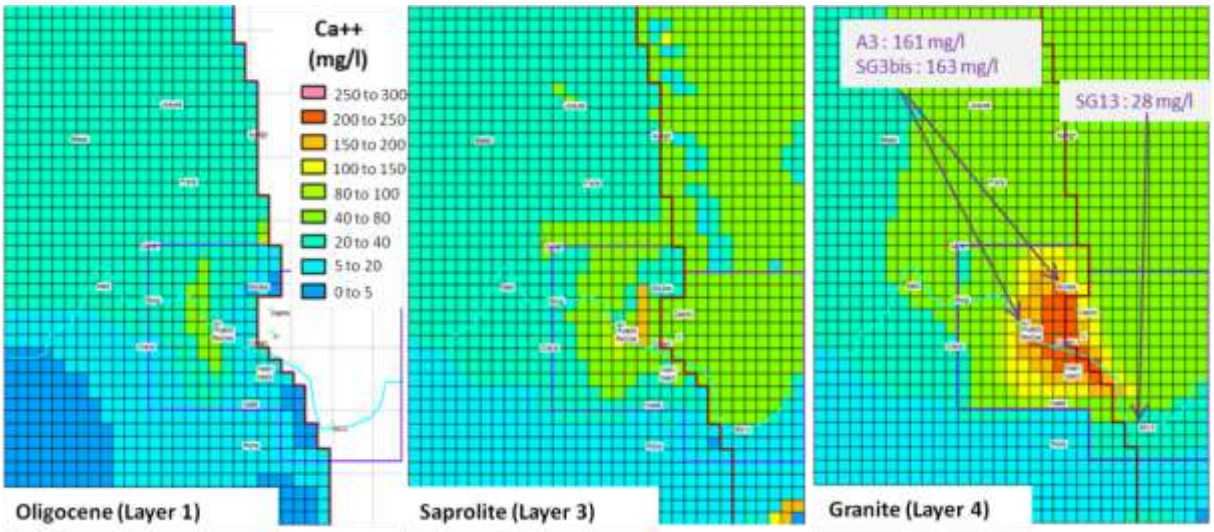

Figure 12: Modelling results: Ca^{2+} content resulting from the mixing and transport of the two poles (i.e. deep pole and dilution pole) in the 3 aquifer layers, from left to right Cenozoic sediments, saprolite and fractured granite. See the location of the modelled area on Figure 9. The observed data are reported in the layer 4.

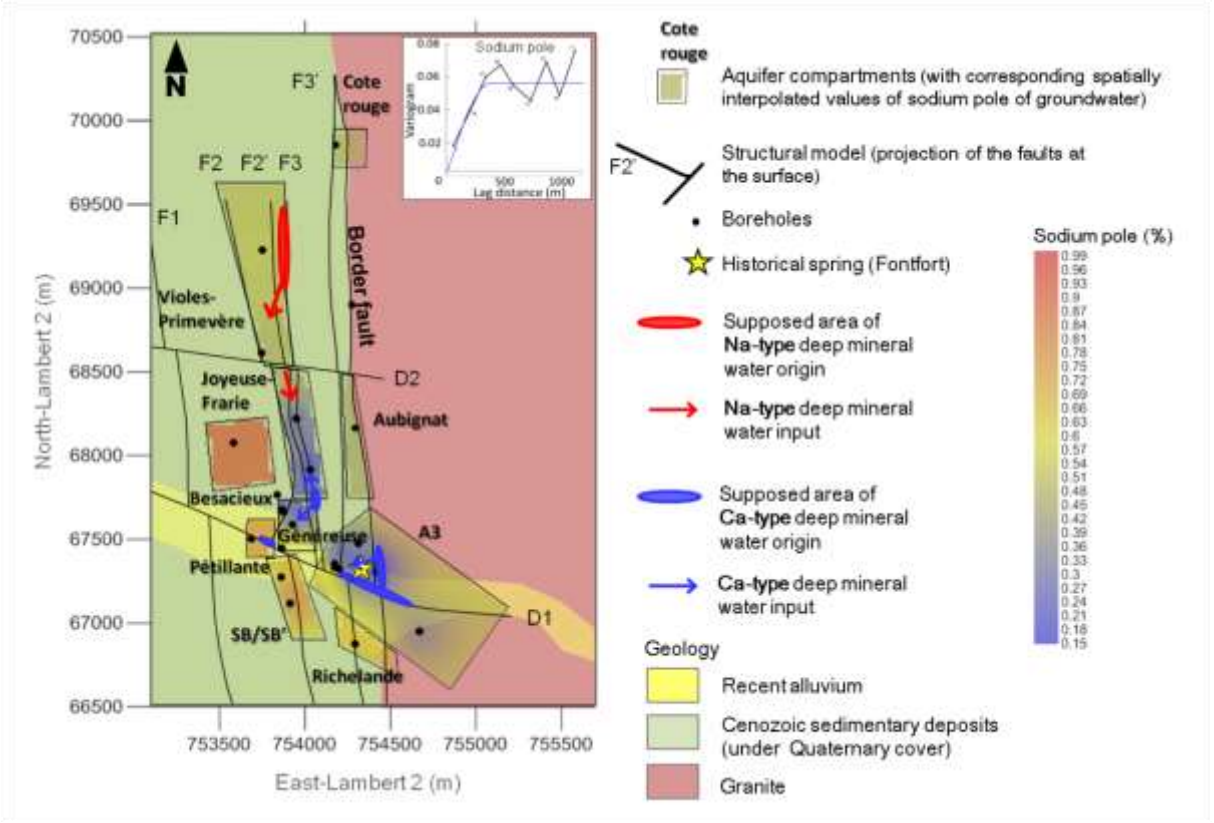

Figure 13: Conceptual model of the Saint-Galmier aquifer system. 10 aquifer compartments were identified (black boxes) with spatial interpolation (kriging) of the sodium pole values. The variogram of the sodium pole is represented in the upper right corner of the map. Impermeable fractures deduced from the structural model are represented by black lines. Few of these structures allow upflowing of Ca-Mg type (blue arrows) and Na-type (red arrows) deep mineralized water (See also Figure 14).

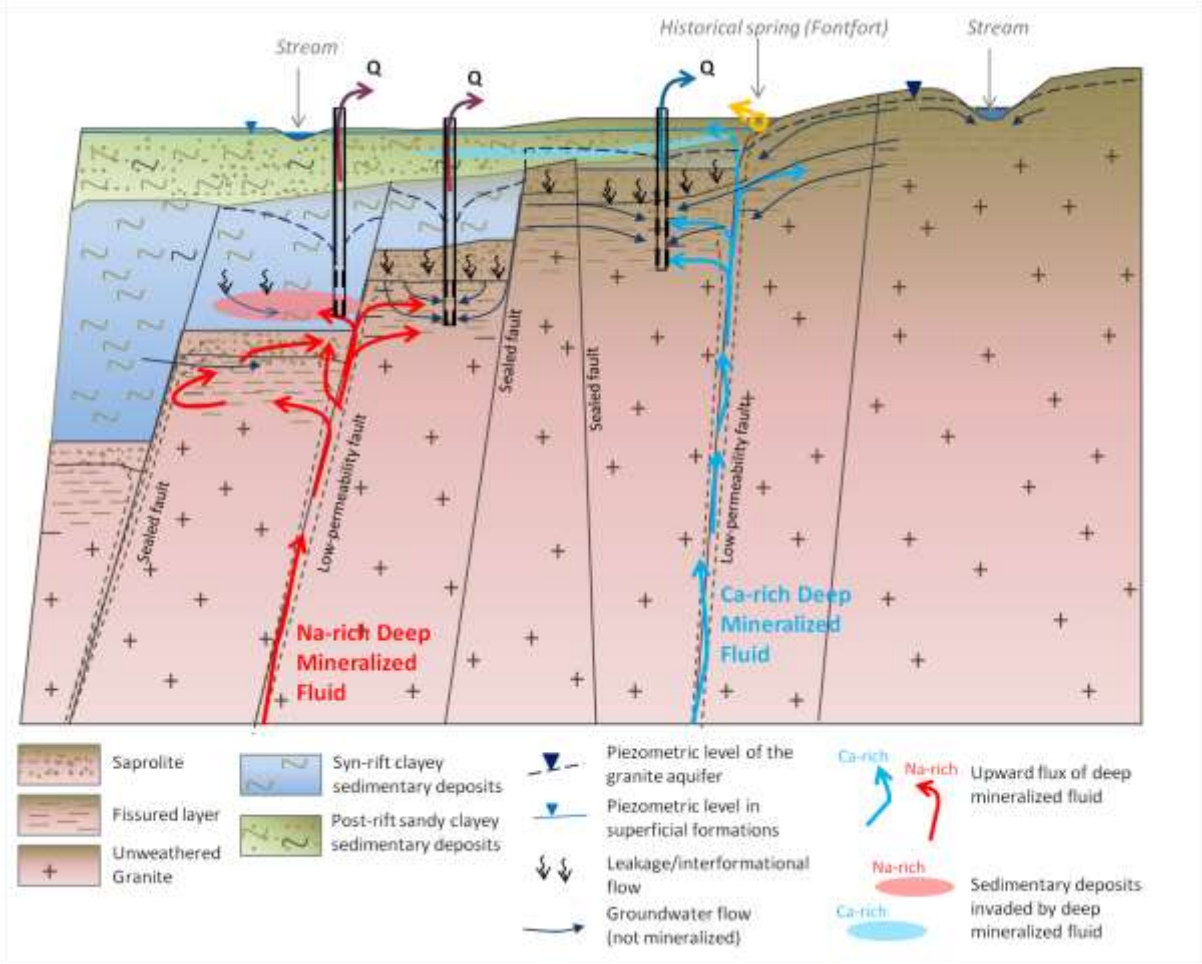

Figure 14: Cross-sectional view (E-W) of the conceptual model of the Saint-Galmier aquifer system.